AD-A047 142 NAVAL POSTGRADUATE SCHOOL MONTEREY CALIF F/G 13/5
A STUDY OF PULL-THROUGH FAILURES OF MECHANICALLY FASTENED JOINT--ETC(U)
SEP 77 R N FREEDMAN

UNCLASSIFIED NL

1 OF 1
ADA047142

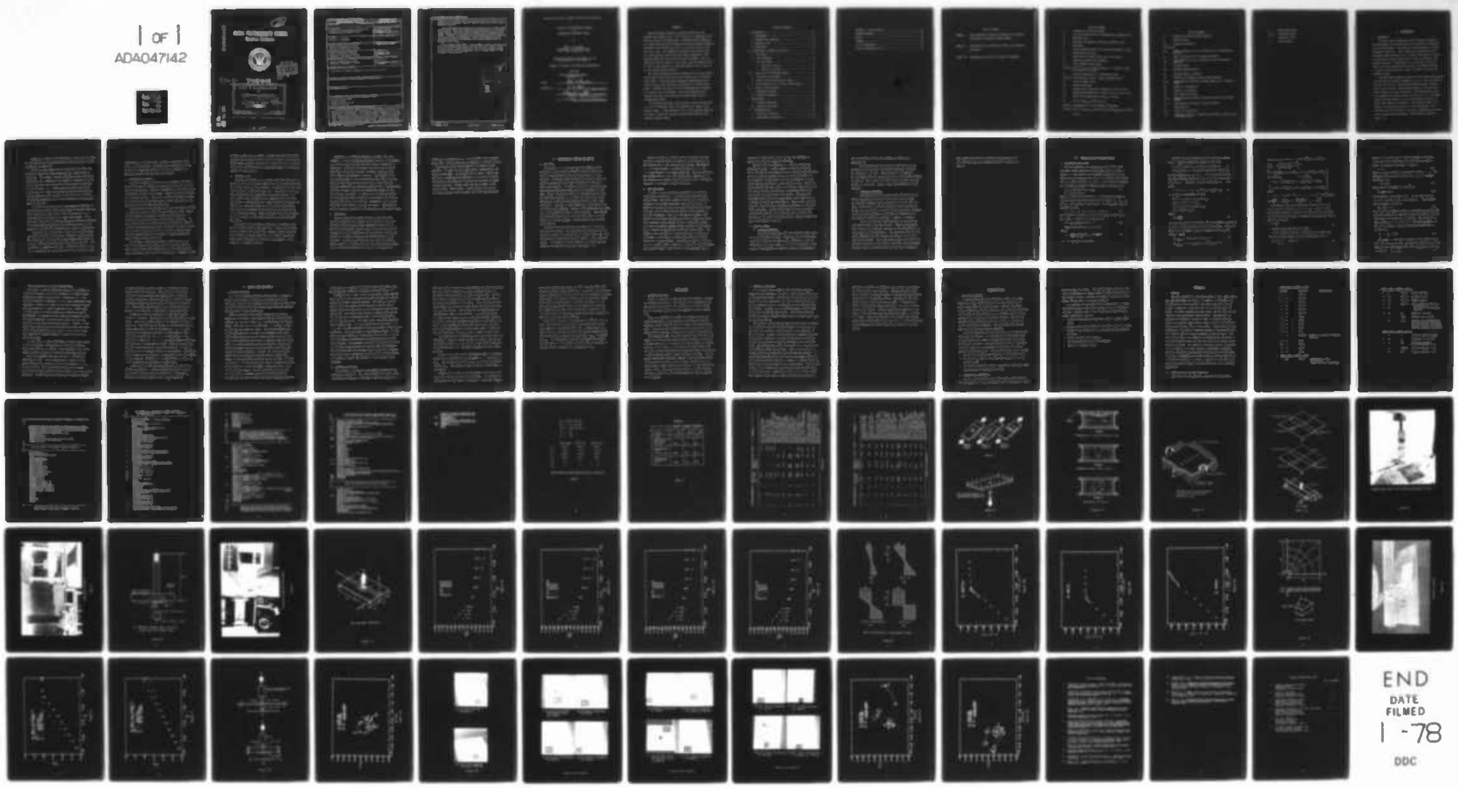

END
DATE
FILMED
1 -78
DDC

1 OF 1

ADA047142

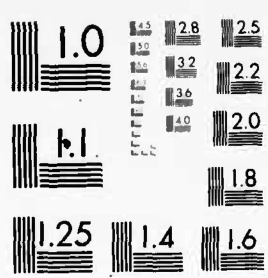


MICROCOPY RESOLUTION TEST CHART
NATIONAL BUREAU OF STANDARDS 1963-A

# NAVAL POSTGRADUATE SCHOOL

Monterey, California



9 Master's

# THESIS

6 A STUDY OF PULL-THROUGH FAILURES

of

MECHANICALLY FASTENED JOINTS.

by

10 Robert N. Freedman 12 80p.

11 Sept[redacted]77

Thesis Advisor: R. E. Ball

Approved for public release; distribution unlimited.



251 450

SECURITY CLASSIFICATION OF THIS PAGE (When Data Entered)

## REPORT DOCUMENTATION PAGE

READ INSTRUCTIONS BEFORE COMPLETING FORM

| | | |
|---|---|---|
| 1. REPORT NUMBER | 2. GOVT ACCESSION NO. | 3. RECIPIENT'S CATALOG NUMBER |
| 4. TITLE (and Subtitle) A Study of Pull-Through Failures of Mechanically Fastened Joints | | 5. TYPE OF REPORT & PERIOD COVERED Master's Thesis; September 1977 |
| | | 6. PERFORMING ORG. REPORT NUMBER |
| 7. AUTHOR(s) Robert N. Freedman | | 8. CONTRACT OR GRANT NUMBER(s) |
| 9. PERFORMING ORGANIZATION NAME AND ADDRESS Naval Postgraduate School Monterey, California 93940 | | 10. PROGRAM ELEMENT, PROJECT, TASK AREA & WORK UNIT NUMBERS |
| 11. CONTROLLING OFFICE NAME AND ADDRESS Naval Postgraduate School Monterey, California 93940 | | 12. REPORT DATE September 1977 |
| | | 13. NUMBER OF PAGES 80 |
| 14. MONITORING AGENCY NAME & ADDRESS(if different from Controlling Office) Naval Postgraduate School Monterey, California 93940 | | 15. SECURITY CLASS. (of this report) Unclassified |
| | | 15a. DECLASSIFICATION/DOWNGRADING SCHEDULE |

16. DISTRIBUTION STATEMENT (of this Report)

Approved for public release; distribution unlimited.

17. DISTRIBUTION STATEMENT (of the abstract entered in Block 20, if different from Report)

18. SUPPLEMENTARY NOTES

19. KEY WORDS (Continue on reverse side if necessary and identify by block number)

through-plane shear
joint failures
fastener pull-through
composite plates

20. ABSTRACT (Continue on reverse side if necessary and identify by block number)

The relationship between the bending moment and the through-plane shear force in the vicinity of a mechanical fastener at failure was determined. Experiments were conducted on 4-inch wide flat plate aluminum and graphite-epoxy composite specimens that modeled portions of a wing skin along a spar and along a rib. The composite specimens were either 8-ply or 16-ply balanced layups and were simply supported at two opposing edges and free along the other two edges. The fasteners were pulled

normal to the plates, and the maximum force at failure was measured for specimen lengths varying from two to six inches between supports.

The aluminum plates failed by formation of a plastic hinge across their width and showed little sensitivity to through-plane shear. The 8-ply spar specimens cracked across their width and also were relatively insensitive to through-plane shear. However, failures of the rib specimens were confined to a region near the fastener, where the fastener pulled through the plate, and showed much greater sensitivity to through-plane shear.

Two analyses were made; one for small elastic deflections of a thin orthotropic plate, and another for a beam in the elastic range. A mesh generator for a finite element model of the plate around the fastener was also developed for the computer program ADINA.

Approved for public release; distribution unlimited.

# A STUDY OF PULL-THROUGH FAILURES
# of
# MECHANICALLY FASTENED JOINTS

by

Robert N. Freedman
Lieutenant, United States Navy
B.A., Miami University, 1970

Submitted in partial fulfillment of the
requirements for the degree of

MASTER OF SCIENCE IN AERONAUTICAL ENGINEERING

from the

NAVAL POSTGRADUATE SCHOOL
September 1977

Author: Robert N. Freedman

Approved by: R E Ball
Thesis Advisor

[illegible]
Chairman, Department of Aeronautics

[illegible]
Dean of Science and Engineering

# ABSTRACT

The relationship between the bending moment and the through-plane shear force in the vicinity of a mechanical fastener at failure was determined. Experiments were conducted on 4-inch wide flat plate aluminum and graphite-epoxy composite speciments that modeled portions of a wing skin along a spar and along a rib. The composite specimens were either 8-ply or 16-ply balanced layups and were simply supported at two opposing edges and free along the other two edges. The fasteners were pulled normal to the plates, and the maximum force at failure was measured for specimen lengths varying from two to six inches between supports.

The aluminum plates failed by formation of a plastic hinge across their width and showed little sensitivity to through-plane shear. The 8-ply spar specimens cracked across their width and also were relatively insensitive to through-plane shear. However, failures of the rib specimens were confined to a region near the fastener, where the fastener pulled through the plate, and showed much greater sensitivity to through-plane shear.

Two analyses were made; one for small elastic deflections of a thin orthotropic plate, and another for a beam in the elastic range. A mesh generator for a finite element model of the plate around the fastener was also developed for the computer program ADINA.

TABLE OF CONTENTS

## LIST OF TABLES

## LIST OF FIGURES

## LIST OF SYMBOLS

| | |
|---|---|
| a | Dimension of plate between supports |
| b | width of plate |
| $D_{ij}$ | flexural rigidities |
| (i,j=1,2,6) | |
| $E_{ij}$ | Young's Modulus in the ij direction for an orthotropic material |
| E | Young's modulus for an isotropic material |
| $G_{ij}$ | Shear modulus in the ij direction for an orthotropic material |
| M | Average moment |
| $M_e$ | Maximum elastic moment |
| $M_f$ | Average moment at failure |
| $M_o$ | Theoretical ultimate elastic-plastic moment |
| $M_{ult}$ | Experimentally obtained ultimate moment for a composite plate |
| $M_x$ | Moment in x direction |
| $M_y$ | Moment in y direction |
| $P_f$ | Pull force at failure |
| $P_{ult}$ | Experimentally obtained ultimate pull force with small moment |
| $P_y$ | Theoretical pull force to cause yielding |
| q | Load applied |
| $Q_y$ | Shear in y direction |
| u,v | Length of sides of a rectangle over which a uniform load is assumed to act |

| | |
|---|---|
| $w$ | plate deflection |
| $x,y,z$ | coordinate axes |
| $\nu$ | Poisson's ratio |
| $\sigma_y$ | Yield stress |

# I. INTRODUCTION

## A. BACKGROUND

In recent years considerable effort has been devoted to the development of new materials for the purpose of improving aircraft performance. One family of these materials is fiber reinforced composites. Many studies have shown that use of advanced composite materials in aircraft structures can result in significant weight savings due to their low density, high modulus character. Furthermore, the anisotropic nature of fiber reinforced composites challenges the aircraft designer to exploit their directional nature in order to realize even greater savings.

Graphite-epoxy composite materials have recently been specified for major structural elements in two U.S. Navy and Marine aircraft currently in advanced development stages. Specifically, the wing skin, leading edge extension, trailing edge flap, rudder, horizontal stabilizer, and vertical fin are to be constructed of graphite-epoxy in the F-18, [1]. The underlying wing substructure is to be constructed of metal in a traditional spar-rib arrangement. The second aircraft, the AV-8B, is the advanced version of the AV-8 Harrier. This aircraft will have the entire wing box, consisting of the skin and the torque box substructure, constructed of graphite-epoxy, [2]

Mechanical fasteners are specified to attach the wing skins to the underlying wing substructure for both aircraft to allow removal of the skins,[3].

Extensive tests under various conditions have been conducted to assess the risks associated with graphite-epoxy materials. For example, strength degradation due to moisture absorption, high temperature environments, galvanic corrosion, and fatigue have been determined for the service environment of both aircraft, [3]. These tests have shown that design strain levels for both the Harrier and the F-18 wing designs provide adequate safety margins for the detrimental effects of elevated temperature and moisture absorption to be encountered in service.

In addition to the ability of the composite structure to withstand design loads under a wide range of service conditions, some attention has been given to the vulnerability of aircraft composite structures in a combat environment. Tests have been conducted to study the response of advanced composites to ballistic impact damage and the concomitant reduction in strength. A discussion of these tests is given in Reference [4].

Much data are available and a great deal is known about the behavior of metals at failure. Theories of failure have been tested time and again and failure models have proven valuable in predicting stress levels that lead to failure. With the advent of composite materials, attempts to model the behavior of composites and the failure mechanisms have led to some

understanding of failure modes. However, significant gaps exist in the literature. Of particular interest here is the failure of a composite structure at a metal fastener in a particular mode called fastener pull-through.

## B. FASTENER PULL-THROUGH

Consider a composite plate or skin fastened to the underlying structure with mechanical fasteners, as in the F-18 and Harrier wing designs. Primary considerations in selecting skin thicknesses include in-plane shear, tensile strength and critical buckling stresses. Joints are primarily designed to transfer in-plane tensile and compressive loads in the skin to the underlying spar-stiffener-rib structure.

Three different failure modes at a joint are shown in Figure 1. These are bearing, shear-out, and tensile failure. These failure modes are discussed in detail in Reference [5]. A fourth type of joint failure is illustrated in Figure 2. In this failure mode the fastener is pulled through the plate by a large through-plane shear force. Although very little attention has been given to this type of failure in metals, this failure mechanism may be significant in fibrous composites under certain loading conditions.

For example, through-plane shear stress exists in the skin of pressurized fuel tanks. Strain levels are usually small under normal design conditions, and the through-plane shear stresses at the joint are insignificant. However, if the

aircraft takes a hit in combat, circumstances may arise which subject joints around the fuel tanks to unusually high through-plane shear stresses. The extent to which the joint is able to carry these stresses may have significant impact on the vulnerability of the aircraft.

## C. HYDRAULIC RAM

Consider the problem of an integral wing fuel tank which is partially full of fluid when impacted by a high speed projectile. The kinetic energy of the projectile is transferred to the fluid in the tank as it passes through, [6]. The result of this energy transfer has been characterized by three phases. The first phase is the propagation of a shock through the fluid. The second is the formation of a vapor filled cavity behind the projectile. The third phase is an oscillatory phase during which the cavity expands and contracts as the system returns to an equilibrium state. These phenomena, illustrated schematically in Figure 3, have been referred to as the hydraulic ram effect.

The intense fluid pressure created by the hydraulic ram has a two-fold effect on the tank wall. First, the pressure, acting perpendicular to the wall, creates a moment distribution through the plate. Secondly, the through-plane shear forces that arise must be reacted by the fasteners. This situation is shown in Figure 4.

Reference [7] describes hydraulic ram tests that were conducted on fluid containing aluminum tanks and one manifestation of the failure of the tank walls was an "unzipping" of fasteners. Although the fasteners that were used in these tests were not typical aircraft fasteners, questions were raised about such connection failures. If aluminum plates and rivets failed in this through-plane mode, then it may be possible that composite plates will fail in the same way. Although composites are generally pound-for-pound stronger than aluminum in-plane, they may be considerably weaker in the through-plane direction. In addition to the bending moment and through-plane shear induced by the hydraulic ram loading, aircraft skins will be in tension, compression, and in-plane shear due to maneuvering when the hit occurs. This combination of stresses can lead to a significantly lower failure load.

## D. OBJECTIVES

Several aluminum and graphite-epoxy plates have been tested to determine the sensitivity of failure to the combination of through-plane shear and bending moment due to hydraulic ram loading. Specifically, the objectives were to determine the force required to pull a fastener through the plates for a range of values of the bending moment at the fastener. A failure curve relating pull force and bending moment similar to a yield curve for limit analysis was sought. Since reinforcing fibers do not run in the through-plane

direction in composite plates, it was expected that through-plane shear strength would be low compared to aluminum plates.

Macroscopic failure mechanisms in both materials were observed. In order to verify experimental observations, two analyses were made. One analysis was for small, elastic deflections to determine the magnitude of the errors in moment distribution associated with treating the specimens as beams instead of plates. Another model applies to beams in the plastic range. Additionally, a mesh generator for use in the elastic-plastic finite element code ADINA was developed.

## II. EXPERIMENTAL APPROACH AND SET-UP

### A. THE MODEL

From Figure 4 it is apparent that the hydraulic ram loading on a plate creates a complex internal stress distribution throughout the plate and particularly at the fastener. To further complicate matters, hydraulic ram is a dynamic problem involving large pressures applied over a short time interval. In order to facilitate the experimental and analytical approach, some simplifying assumptions were made. First, the dynamic effects of the hydraulic ram were not addressed, although it is known that they are of great importance in inducing catastrophic failures at fuel tank boundaries. Secondly, it was assumed that there would be no in-plane stresses present. Again, it was recognized that these will play an important role in joint failures. These assumptions are justified here on the basis that this is a first study in an ongoing program. Future studies will consider these effects.

Figures 5A and 5B illustrate the modeling of the skin with the test plates. The underlying structure may be envisioned as either a rib, Figure 5A, or a spar, Figure 5B. The difference has importance only with respect to the composite plates. For example, the zero degree ply direction was assumed to run parallel to the main wing spars, [1].

Figure 5C shows the loading set-up to simulate the combination of bending moment and shearing force that exist at the fastener due to the hydraulic ram loading. The edges at $y = \pm b/2$ were assumed to be free and those at $x = 0$ and $x = a$ were assumed to be simply supported. The free condition was assumed because, near the ribs and spars, moments due to the hydraulic ram loading would be smaller in the y direction compared to the moments in the x direction.

## B. TEST EQUIPMENT

In order to load a specimen as suggested by Figure 5C, a devide was constructed in the Naval Postgraduate School Machine Shop. The simple support condition was provided by triangular knife edges fashioned from steel bar stock. A means was provided by which the supports could be positioned from one to five inches from the center of the specimen in one-inch increments. By moving the supports outward, the moment at the fastener becomes larger for a given pull force. Thus, supports close together provide a relatively larger pull force and smaller moment whereas supports farther apart give a relatively smaller pull force and larger moment. The supports were attached to a rigid steel base to facilitate attachment of the device to the moveable head of a Riehle 200,000 lb. testing machine. The device is shown in Figure 6 with an aluminum plate in place for a test pull. The fasteners were passed through a hole drilled in the specimens and at-

tached to a Clevis device which in turn was attached to a Baldwin SR-4 5000 lb. capacity load cell.

The load cell was connected to a locally constructed wheatstone bridge. A power supply and digital voltmeter were connected to the bridge circuit in the usual way and calibrated to read an integer multiple of the load applied at the fastener. Bridge output was also monitored on a strip-chart recorder calibrated to read pounds of pull. The strip-chart recorder was most useful in providing a time history of the applied loading and assisted in recording significant events which occurred during the loading. Some aluminum specimens were fitted with strain gauges, which were wired to a wheatstone bridge switching device. Gauge output was monitored by a second digital voltmeter calibrated to read micro-inches per inch. An additional channel of the strip-chart recorder was available to monitor the strain gauge output selected at the manual switching station. Figure 7 shows the entire experimental facility.

## C. TEST SPECIMENS

### 1. Aluminum Specimens

The aluminum specimens were machined from sheet stock to a four-inch nominal width. Lengths of the specimens were varied from seven to fourteen inches, depending on the intended location of the supports. A hole was machined in the center of the specimen to provide a nominal two-thousandths

inch interference fit for the fastener as specified in Reference [8].

The fasteners that were used for the tests are the Hi-Tigue Hiloks that have been specified as skin fasteners for portions of the F-18. These HLT-328-8-18 fasteners are often specified for applications which require high fatigue resistance. Their unique Hi-Tigue feature, however, was not germane to the tests. Figure 8 shows the dimensions of the fastener.

2. Composite Specimens

The composite plate specimens were fabricated by the author from Hercules AS-3501-6 twelve-inch pre-preg tape. The tape was a nominal ten mil thickness with low resin content. Five 16-inch x 16-inch plates were constructed using either 8-ply $[0/\pm45/90]_s$ or 16-ply $[0/\pm45/0_2/\pm45/90]_s$ balanced layups and were prepared in accordance with Reference [9]. The composite preparation equipment is shown in Figure 9.

Four-inch wide test specimens were cut from the 16-inch square plates after post-curing. Some 8-ply specimens were prepared such that the 0-degree ply was perpendicular to their axis (the spar specimens). The remaining 8-ply and the 16-ply specimens had the 0-degree ply parallel to the axis (the rib specimens). The plates were drilled and fitted with the same fasteners as the aluminum specimens, although interference fitting is not specified for this type of material.

Room temperature material properties from Reference [5] are tabulated along with computed flexural rigidities in Table I.

# III. ANALYTICAL AND COMPUTER MODELS

## A. ANALYTICAL PLATE MODEL

The test specimens are idealized as thin plates with two edges simply supported and two edges free, as shown in Figure 10. The deflections and moment distribution can be approximated by assuming the load to be uniformly distributed over the shaded rectangle of area uv. The governing equation for a balanced, symmetric laminated plate is given by [6].

$$D_{11}w_{,xxxx}+2(D_{12}+2D_{66})w_{,xxyy} \qquad (1)$$
$$+D_{22}w_{,yyyy}=q(x,y)$$

where $w$ is the plate deflection, $q$ is the applied pressure load and subscripts denote partial derivatives. $D_{11}$, $D_{12}$, $D_{22}$, and $D_{66}$ are stiffness coefficients. In the special case of isotropy we have,

$$D_{11} = D_{22} = D; \quad D_{12} = \upsilon D; \quad D_{66} = D(1-\upsilon)/2 \qquad (2)$$

The solution to Equation (1) for the portion of the plate prst shown in Figure 10 is given by [9].

$$w = \sum_{m=1,3,\ldots}^{\infty} \{(a_m+A_m\cosh(m\pi y/a) + \qquad (3)$$
$$+B_m(m\pi y/a)\sinh(m\pi y/a)\} \sin(m\pi x/a)$$

where,

$$a_m = \frac{4Pa^4(-1)^{(m-1)/2}}{\pi^5 m^5 D_{11}uv} \sin\left(\frac{m\pi u}{2a}\right) \qquad (4)$$

and a is the span of the plate.

Considering the unloaded portion of the plate beyond line ts , assume a deflection surface of the form,

$$w^1 = \Sigma\{A^1{}_m \cosh(m\pi y/a) + B^1{}_m (m\pi y/a)\sinh(m\pi y/a) \tag{5}$$

$$+ C^1{}_m \sinh(m\pi y/a) + D^1{}_m (m\pi y/a)\cosh(m\pi y/a)\}\ \sin(m\pi x/a)$$

The six constants $A_m$, $B_m$, $A^1{}_m$, ....$D^1{}_m$, must satisfy the free edge boundary conditions at $y = b/2$, and continuity along line ts . Applying continuity conditions at $y = b/2$ gives

$$w = w^1;\ w_{,x} = w^1{}_{,x};\ w_{,xx} = h^1{}_{,xx};\ w_{,xxx} = w^1{}_{,xxx} \tag{6}$$

It is shown in Reference [9] that

$$A_m - A^1{}_m = a_m(\gamma_m \sinh 2\gamma_m - \cosh 2\gamma_m) \tag{7}$$

$$B_m - B^1{}_m = a_m/2\ (\cosh 2\gamma_m)$$

$$C^1{}_m = a_m(\gamma_m \cosh 2\gamma_m - \sinh 2\gamma_m)$$

$$D^1{}_m = a_m \sinh 2\gamma_m)/2$$

where

$$\gamma m = \frac{m\pi v}{4a} \tag{8}$$

Two more equations are available from the boundary conditions at $y=b/2$ in order to solve for the six constants. Along the edge $y=b/2$ the moment $M_y$ and the shearing force $Q_y$ must vanish. Hence

$$M_y \Big|_{y=b/2} = -(D_{22}w_{,yy} + D_{12}w_{,xx}) = 0 \tag{9}$$

$$Q_y \Big|_{y=b/2} = -(D_{22}w_{,yyy} + (D_{12} + 2\ D_{66})w_{,xxy}) = 0$$

Substitution of Equation (4) into Equation (9) gives,

$$\begin{Bmatrix} A^1{}_m \\ B^1{}_m \end{Bmatrix} = \left( \frac{4\ Pa^4 (-1)^{(m-1)/2}}{m^5 \pi^5 D_{11} uvK} \right) x$$

$$\begin{bmatrix} (1-\rho_2)\alpha_m \cosh\alpha_m - (\rho_2 - 3)\sinh\alpha_m & (\rho_1 - 1)\alpha_m \sinh\alpha_m - 2\cosh\alpha_m \\ (\rho_2 - 1)\sinh\alpha_m & (1-\rho_1)\cosh\alpha_m \end{bmatrix}$$

$$x \begin{Bmatrix} -C^1{}_m (1-\rho_1)\sinh\alpha_m - D^1{}_m (\ (1-\rho_1)\alpha_m \cosh\alpha_m + 2\sinh\alpha_m) \\ -C^1{}_m (1-\rho_2)\cosh\alpha_m - D^1{}_m (\ (1-\rho_2)\alpha_m \sinh\alpha_m - (\rho_2 - 3)\cosh\alpha_m) \end{Bmatrix}$$

where

$$\kappa = (1-\rho_1)\ (1-\rho_2)\alpha_m + [2(\rho_2 - 1) + (\rho_1 - 1)\ (\rho_2 - 3)]\ \cosh\alpha_m \sinh\alpha_m$$

$$\alpha_m = \frac{m\pi b}{2a}\ ; \rho_1 = \frac{D_{12}}{D_{22}};\ \rho_2 = \frac{(D_{12} + 2D_{66})}{D_{22}};\ \rho_3 = \frac{D_{12}}{D_{11}}$$

The quantity that is of particular interest here is the distribution of M along the line $x = a/2$. A plot of $M_x/M$ versus $2y/b$ is shown in Figure 11 for the aluminum specimen, and each of the three types of composite specimens for various values of a, where

$$M = \frac{Pa}{4} \tag{11}$$

B. PLASTIC LIMIT ANALYSIS FOR A BEAM

If the aluminum specimen is considered as a beam, then the total bending moment is given by Reference [12] as

$$M = b \int_{-t/2}^{t/2} z\sigma(x)\ dz \tag{12}$$

Where b is the width and t is the thickness of the beam. Making the usual assumptions that plane sections remain plane, the strain at any point is given by

$$\varepsilon = \kappa z \tag{13}$$

Where $\kappa$ is the curvature of the middle surface, $z = 0$. For moments below a certain critical value, $M_e$, all stresses are elastic and

$$= E\varepsilon = E\kappa z \tag{14}$$

Substituting into Equation (12) gives

$$M = \frac{1}{12}\, b\, E\kappa t^3 \tag{15}$$

If the moment is increased until at the outer fibers, $z = \pm t/2$, is equal to the yield stress, $\sigma_y$, the maximum elastic moment is given by

$$M_e = \frac{1}{6}\, b\, t^2 \sigma_y \tag{16}$$

Since only the outermost fibers of the beam are yielded, the beam will continue to carry additional load through the central fibers until they too are yielded. The situation is shown schematically in Figure 12. The limiting moment is Case (D) of Figure 12 where the entire cross section is yielded and,

$$M_o = \frac{1}{4}\sigma_y\, bt^2 \tag{17}$$

The moment in the beam is largest at the center of the span and its value is Pa/4. Substituting Equation (11) into Equation (17), the maximum pull that the beam can carry, $P_y$, is given by

$$P_y = \sigma_y \frac{b}{a} t^2 \tag{18}$$

## C. MESH GENERATOR FOR A FINITE ELEMENT MODEL

The theory of matrix structural analysis is discussed at length in Reference [13], and a discussion of various three-dimensional elements can be found in Reference [14]. The studies presented in Reference [14] by Clough demonstrate that hexahedral elements with nodes on the sides adequately represent the bending of a simply supported plate. Clough used a single layer of 20 node elements and achieved the exact deflections. He showed that more complicated elements, such as curved tetrahedra, could perform as well, but that the formulation time was significantly greater. Further, it was shown that, while two-point Gauss quadrature rules gave exact results for rectangular prisms, three- or four-point rules were required for skewed elements in order to achieve the desired accuracy.

In this study, 16 node isoparametric elements were chosen to model specimens. The objective of the finite element effort was primarily to develop a mesh generator which could later be used to analyze the laminated anisotropic plates.

The finite element code used was ADINA, developed by Bathe [15] in 1975. ADINA incorporates a library of four basic elements and allows selection of any combination of 15 material models. The library material model that seemed best suited was the isotropic elastic-plastic model with strain hardening. Tensile tests were conducted on aluminum coupons

of three different alloys in order to accurately provide proper input data for ADINA. The results of the tensile tests were used throughout the investigation as baseline material properties, and the stress strain curves for three different aluminum alloys are shown in Figures 13A through 13C. The bilinear approximation to the stress strain behavior of the materials is indicated by the broken lines.

Symmetry of the test specimens allowed some simplification of the model. The analysis includes one-quarter of the plate. The finite element model of the specimen is shown in Figure 14. The loads can be applied as concentrated loads at nodes along lines (A) and (B) of Figure 14. At $x = 0$, restraints can be applied such that no displacement in the $x$ direction is permitted. At $y = 0$, no displacement in the $y$ direction is permitted. At $x = a$, the simple support condition dictates that no displacement in the $z$ direction is permitted. The only other constraints involve the nodes at $z = 0$ and on the first ring of elements closest to the fastener. The assumption is made that the fastener is essentially rigid with respect to the aluminum. Consequently, no displacement in either the $x$ or $y$ directions is permitted for these nodes.

A description of the mesh generator, and its use is included in Appendix A. Present limitations internal to the ADINA source code preclude the possibility of obtaining a successful nonlinear analysis due to array dimension.

## IV. RESULTS AND DISCUSSION

### A. ALUMINUM SPECIMENS

All of the aluminum specimens tested failed by forming a plastic hinge across the center of the span, as shown in Figure 15. None of the fasteners pulled through, and there was no visual indication that the through-plane shearing stresses had any effect on the failure mode.

Table II contains the ultimate moment and pull force based upon the plastic limit analysis and the actual maximum moments, $M_f$, and pull forces, $P_f$, obtained during the experiments. Note that due to the fact that a = 4 inches, $P_f$ and $M_f$ have the same numerical value. The ultimate moments obtained experimentally are seen to be somewhat higher than those predicted by the plastic limit analysis of section III. Part of the difference may be due to the fact that the theory applies to elastic-perfectly plastic materials, whereas the materials tested (particularly the AL7075T6) exhibited some degree of strain hardening. Further, the limiting moments predicted by the theory are average moments, whereas the moment is not distributed uniformly across the beam, as shown in Figure 11. If the ultimate pull force is taken to be that force required to raise the moment M along the Line $x = a/2$ to the ultimate moment, then the predicted values of pull, $P_f$, more closely resemble those obtained experimentally. In any case, the tests indicate that these aluminum plates fail

at the joint in a plastic hinge mode. This hinge effect has previously been observed in hydraulic ram experiments, [7].

Figures 16 and 17 show a plot of the stress versus applied load for two of the locations which were provided with strain gauges on the 6061 aluminum specimen. The stress is normalized by the yield stress for the material, and the load is normalized by the theoretical $P_f$ for the material and support conditions. The figures also contain the theoretical stress for a beam with a concentrated load of the same magnitude, and for the flat plate. For these tests, the simple supports were 4 inches apart. It can be seen that at the point $x = 2$, $y = 1.040$, the beam approximation does not predict stress levels accurately. The plate theory is considerably better. Further away from the centerline of the plate, at $x = 2.735$, $y = .735$, the plate theory overestimates the experimentally obtained stress levels. This suggests the possibility that formulation of the plate problem may not be accurate near the fastener. The assumption that the fastener head behaves like a uniform load acting over a rectangular area may not be refined enough to accurately predict the stresses in the vicinity of the fastener.

## B. COMPOSITE SPECIMENS

The results of all tests on the composite specimens are presented in Table III. $M_{ult}$ was determined for each of the five plates by applying a line load across the center of a

four-inch wide by seven-inch long specimen cut from each plate. The line load was applied by a steel cylinder attached to the Riehle testing machine, as shown in Figure 18A. The fastener passes through a hole in the cylinder and the hole in the plate and attaches to the clevis. Thus, pulling the fastener causes the cylinder to bear against the plate along the axis of the cylinder. This eliminates the concentration of through-plane shear at the fastener. $P_{ult}$ was determined for each 16-inch square plate by pulling a fastener through a two-inch by two-inch specimen restrained by a two-inch by six-inch by five-eighths-inch thick steel plate with a circular hole eighty-thousandths of an inch larger than the radius of the fastener head. The $P_{ult}$ set-up is shown in Figure 18B.

Two complete sets of experiments were run on the 8-ply rib specimens in order to establish that the results were not attributable to defects in the quality of the plates from which the specimens were cut. The mean difference was less than 7 percent.

Figure 19 is a plot of the experimental data in nondimensional form. The abscissa is the moment, M, normalized by $M_{ult}$. The ordinate is the pull force at failure, $P_f$, normalized by $P_{ult}$. The extent or mode of failure is indicated in the figure.

Figures 20A-20L consist of photographs of the 8-ply spar, 8-ply rib, and 16-ply rib failed specimens. The sequence of photographs for each group of specimens is from small moment

and mostly through-plane shear, to small through-plane shear and mostly moment loading conditions. The extent of the failure zone is indicative of the sensitivity of the specimen to through-plane shear. Note that the failure zone for specimens loaded with relatively small moment is primarily confined to a region around the fastener hole. As the moment was increased (by lengthening the span) this failure zone extended in the $y$ direction until it covered the entire width and resembled the failure of the line loaded specimen.

Figure 21A is a plot of the data from a different point of view. The abscissa in this plot is the theoretical elastic local moment at the fastener head, $M_{ult}$, normalized by $M_{ult}$. Figure 21B is a plot of the theoretical elastic moment at the edge of the plate at the center of the span, $M_{edge}$, normalized by $M_{ult}$. The theoretical values were obtained from Figures 11A and 11B at $y = 0.4$ inches. In both cases the ordinate is the pull force at Failure, $P_f$, normalized by $P_{ult}$.

# V. CONCLUSIONS

## A. ALUMINUM SPECIMENS

It was not possible to pull the HL-328-8 fasteners through the aluminum test plates. The failure of the aluminum joints was manifested entirely by the formation of a plastic hinge and the resultant inability of the specimen to carry further load.

There is essentially no comparison between the way the aluminum specimens and the composite specimens failed when subjected to the combined effects of moment and through-plane shear. Failure of the aluminum plates was insensitive to the through-plane shear force induced by the head of the fastener.

The assumption that the plates behaved like beams when subjected to a force on the fastener does not appear to be valid, with the exception of the special case where moment (or support spacing) is very large. It was shown from plate theory that the effect of the concentrated load upon the moment distribution is more significant where support spacings are small. The approach taken here, therefore, requires some refinement before it can accurately predict stress levels. However, use of a finite element model should allow designers to more accurately predict stress levels that lead to failure. A wide variety of loading conditions and fastener geometries may be studied in this manner.

B. COMPOSITE SPECIMENS

It is evident from Figure 20 that the weaklv-oriented composite spar specimens, 52 and 53, were largely insensitive to through-plane shear. The location of the failure points on Figure 19 is also indicative of a lack of sensitivity since these specimens failed at a load that was very near the ultimate moment. However, the rib specimen showed a significant sensitivity to through-plane shear. The thickest specimens showed the greatest degree of sensitivity, and this result may be cause for concern.

The manner in which pull-through failure occurs is complex. It is suspected that the ultimate moment is attained over an area near the fastener, causing failure of the specimen in that vicinity. However, the distribution of moments over the centerline is such that a portion of the plate outside this failure zone maintains sufficient strength to carry further load. The through-plane shear forces must still be carried by the composite around the fastener. Thus, as the load is increased further, the fastener pulls through the specimen. In those specimens which were loaded with large moment and small pull-through, the distribution of moments is flatter along the centerline, since the supports are further apart. That is, the effect of the concentrated load induced by the fastener head is less pronounced. Conseuqnetly, once local failure around the fastener occurs, only a small increase in pull force is

required to increase the moment to its critical value along the entire width of the specimen. Thicker and wider specimens, in which the ultimate moment is larger, may show greater sensitivity to through-plane forces, and therefore be less likely to fail across their entire width. It would be in thick, stiff materials where "unzipping," if it is to occur, would be most likely. Current wing design concepts for portions of the F-18 wing call for thicknesses from .3 to about 0.7 inches. Clearly, as thickness gets larger, the through-plane shear strength gets larger and there is a point where the actual through-plane shear loads can be carried by the composite.

# VI. RECOMMENDATIONS

## A. ANALYTICAL METHODS

A mesh generator has been developed to model the simply supported- simply supported-free-free plate loaded over a small region under the fastener head. This has been done using an elementary loading condition and an isotropic material. A great deal of understanding could be gained if the program were modified to include orthotropic elements. The current program allows generation of up to 16 layers of 16-node isotropic isoparametric elements. The node generation and element connectivity would remain unchanged.

A further sophistication could be realized by treating the nodes near the fastener as fixed and applying pressure loads as predicted by the computer program Satans [16]. Satans has the ability to predict pressure distributions on a plate that arise in a fluid as a consequence of hydraulic ram from a specific threat projectile. Other modifications could include:

1. The ability to change the geometry of the fastener head.
2. The ability to take into account the flexibility of the fastener head.
3. Inclusion of in-plane tensile, compression, and shear loads characteristic of maneuvering flight.

## B. EXPERIMENTAL PROCEDURES

No data were obtained at the lower moment ranges because of the inability to move the support arms of the machine closer

together than two inches. This design defect should be corrected by affixing the support arms to a base which permits a full range of motion, and does not restrict selection of distances between arms to one inch increments.

Investigation of the sensitivity of composites to a more complicated stress state which includes in-plane stresses is required. Further study is also required on factors which affect sensitivity, such as:

1. Fastener head geometry variations, such as counter-sunk heads.
2. Fastener-hole buffer materials and seals, such as O-rings.
3. Degree of interference fit or tolerance between fastener and hole.
4. Effects of high cycle fatigue.
5. Existing delaminations or other damage.
6. Effects of softener strips.

# APPENDIX A

## A. GENERAL

The mesh generator is extremely simple to use. Where possible, variable names are exactly the same as in Reference [15]. In addition to the source deck, only four data cards are required to generate a data deck that can be used as input for ADINA. By simply removing the load cards, the deck can also be used with the preprocessor program PSAP1. The generator is specific and therefore limited in that it currently has the ability to generate nodes along 5 radial lines in one quadrant of a plate that has a hole in the center. Other nodes are less restricted. The group of elements closest to the fastener hole are fixed in size by fastener parameters that are input. The size of the rest of the elements is determined by the number of divisions desired along the line that lies at the center of the span of the plate. The capability currently exists to generate up to 16 layers of 16 node isotropic isoparametric elements. However, the source program ADINA requires minor internal modification to accommodate the large volume of storage required by a non-linear analysis. A program is currently underway at the Naval Postgraduate School to provide ADINA with this increased capability.

## B. REQUIRED INPUT FOR MESH GENERATOR

Input data for the generator requires only four cards.

1. Input Card 1 Format (16I5)

| COLUMN | VARIABLE | DESCRIPTION |
|---|---|---|
| 1 - 5 | IDOF(1) | |
| 6 - 10 | IDOF(2) | |
| 11 - 15 | IDOF(3) | |
| 16 - 20 | IDOF(4) | |
| 21 - 25 | IDOF(5) | |
| 26 - 30 | IDOF(6) | |
| 31 - 35 | NEGNL | |
| 36 - 40 | MODEX | |
| 41 - 45 | NSTE | |
| 46 - 50 | IPRI | |
| 51 - 55 | NPB | |
| 56 - 60 | LAYERS | Number of layers of elements desired. |
| 61 - 65 | NEGL | |
| 66 - 70 | NLOAD | |
| 71 - 75 | NLCUR | |
| 76 - 80 | NPTM | |

2. Input Card 2 FORMAT (20A4)

| | | |
|---|---|---|
| 1 - 80 | PTYPE | ALPHANUMERIC TITLE DESIRED ON ADINA AND PSAPI PRINTOUTS. |

3. INPUT CARD 3 FORMAT (8F10.0)

| | | |
|---|---|---|
| 1 - 10 | PROP(1) | Young's Modulus |
| 11 - 20 | PROP(2) | Poisson's Ratio |
| 21 - 30 | PROP(3) | Simple tension |
| 31 - 40 | PROP(4) | Strain Hardening Modulus A Length of |
| 41 - 50 | | half span between simple supports |
| 51 - 60 | R1 | Radius of Fastener |
| 61 - 70 | PMAX | Maximum load desired |
| 71 - 80 | PINC | Desired load increment for load data cards. Different from DT which is load step internal to ADINA, and deals with the method of solution. |

4. INPUT CARD 4 FORMAT (8F10.0)

| | | |
|---|---|---|
| 1 - 10 | R | Radius of Fastener Head |
| 11 - 20 | T | Thickness of specimen |
| 21 - 30 | DT | Loadstep increment Allow to default (0.0) |
| 31 - 40 | TSTART | Allow to default (0.0) |
| 41 - 50 | FAC | Allow to default (0.0) |

```
************************MESH GENERATOR PROGRAM LISTING*******
C
C
C
C
      DIMENSION ANGL(9),ID(3,1500),X(1500),Y(1500),Z(1500),
     *KEL(32,16),KG(32,16),NOD(16,32,16),IPNODE(2,3),IDOF(6),
     *NPAR(20),PROP(4),TIMV(20),RV(20),RV1(20),NODE(1500)
      READ(2,5) (IDOF(I),I=1,6),NEGNL,MCDEX,NSTE,IPRI,NPB,
     *LAYERS,NEGL,NLOAD,NLCUR,NPTM
      READ(2,5) NDIV,IDC, ICON,IPRIC,MAXES
5     FORMAT(16I5)
      READ(2,6) PTYPE
6     FORMAT(20A4)
      READ(2,7) (PROP(I),I=1,4),A,R1,PMAX,PINC
      READ(2,7) R2,T, DT,TSTART,FAC
7     FORMAT(8F10.0)
C
C----------------------------------------------------------------
C
C        ASSIGN VALUES TO CONSTANTS AND SET DEFAULTS
C
C
C----------------------------------------------------------------
C
      NPR=2*NDIV+3
      NPRMID=(NPR+1)/2
      DELR=(A-R2)/FLOAT(2*NDIV)
      N=0
      NODE(1)=00000
      NN=5*NPR+4*NPRMID
      NEL=4*(NDIV+1)
      NDIV1=NDIV+1
      PI=4.0*ATAN(1.0)
      ANGL(1)=0.0
      ANGL(2)=ATAN(.25)
      ANGL(3)=ATAN(.5)
      ANGL(4)=ATAN(.75)
      ANGL(5)=PI/4.0
      ANGL(6)=ATAN(4.0/3.0)
      ANGL(7)=ATAN(2.0)
      ANGL(8)=ATAN(4.0)
      ANGL(9)=PI/2.0
      LAYRS=LAYERS+1
      IPNODE(1,1)=1
      IPNODE(2,1)=NN
      IF(NPB.EQ.2) GO TO 8
      IPNODE(1,3)=NN+1
      IPNODE(2,3)=NN*LAYERS
8     IPNODE(1,2)=NN*LAYERS+1
      IPNODE(2,2)=NN*LAYRS
      IF(NLOAD.EQ.0) NLOAD=23
      IF(NLCUR.EQ.0) NLCUR=2
      IF(NPTM.EQ.0) NPTM=NSTE
      MTYP=1
      IELD=0
      IELX=0
      IST=0
      IDIRN=1
      NPTS=NPTM
      NTF1=1
      NTF2=2
C
C----------------------------------------------------------------
C
C              GENERATE THE NODAL MESH, LAYER BY LAYER
C              EACH ELEMENT WILL HAVE 16 NODES, 8 ON THE
```

```
C          Y-Z UPPER AND 8 ON THE Y-Z LOWER SURFACE.
C            NO NODES ARE GENERATED THROUGH THE THICKNESS
C            OF THE ELEMENT.
C
C-----------------------------------------------------------------
C
          DO 50 K=1,LAYRS
          XN=T*(1.0-FLOAT(K-1)/FLOAT(LAYERS))
          DO 40 J=1,9
          THETA=ANGL(J)
          IF(MOD(J,2).EQ.0) GO TO 21
          DO 31 I= 1,NPR
          N=N+1
          IF(N.NE.1) NODE(N)=NODE(N-1)+1
          IF(N.EQ.1) NODE(1)=1
          ID(1,N)=0
          ID(2,N)=0
          ID(3,N)=0
          IF(J.EQ.1)ID(3,N)=1
          IF(J.EQ.9)ID(2,N)=1
          IF(J.GE.5.AND.I.EQ.NPR)ID(1,N)=1
          IF(K.NE.LAYRS) GO TO 15
          IF(I.EQ.1) ID(2,N)=1
          IF(I.EQ.1)ID(3,N)=1
15        X(N)=XN
          IF(I.NE.1) GO TO 16
          Y(N)=R1*COS(THETA)
          Z(N)=R1*SIN(THETA)
          GO TO 30
16        IF(I.NE.2) GO TO 17
          Y(N)= (R1+(R2-R1)/2.0)*COS(THETA)
          Z(N)=(R1+(R2-R1)/2.0)*SIN(THETA)
          GO TO 30
17        IF(I.NE.3) GO TO 18
          Y(N)=R2*COS(THETA)
          Z(N)=R2*SIN(THETA)
          GO TO 30
18        IF(I.EQ.NPR) GO TO 19
          Y(N)=(R2+FLOAT(I-3)*DELR)*COS(THETA)
          Z(N)=(R2+FLOAT(I-3)*DELR)*SIN(THETA)
          GO TO 30
19        IF(J.GT.5) GO TO 20
          Y(N)=A
          Z(N)=A*TAN(THETA)
          GO TO 30
20        Y(N)=A*COTAN(THETA)
          Z(N)=A
30        IF(J.EQ.9)Y(N)=0.0
31        CONTINUE
          GO TO 40
21        DO 33 I=1,NPRMID
          N=N+1
          NDINC=2
          IF(I.EQ.1)NDINC=1
          NODE(N)=NODE(N-1)+1
          ID(1,N)=0
          ID(2,N)=0
          ID(3,N)=0
          IF(J.GE.5.AND.I.EQ.NPRMID)ID(1,N)=1
          IF(K.EQ.LAYRS.AND.I.EQ.1)ID(2,N)=1
          ID(3,N)=ID(2,N)
          X(N)=XN
          IF(I.NE.1)GO TO 22
          Y(N)=R1*COS(THETA)
          Z(N)=R1*SIN(THETA)
          GO TO 32
22        IF(I.NE.2)GO TO 23
          Y(N)=R2*COS(THETA)
          Z(N)=R2*SIN(THETA)
          GO TO 32
23        IF(I.EQ.NPRMID) GO TO 24
          Y(N)=(R2+FLOAT(I-2)*2.0*DELR)*COS(THETA)
          Z(N)=(R2+FLOAT(I-2)*2.0*DELR)*SIN(THETA)
```

```
      GO TO 32
24    IF(J.GT.5)GO TO 25
      Y(N)=A
      Z(N)=A*TAN(THETA)
      GO TO 32
25    Y(N)=A*COTAN(THETA)
      Z(N)=A
32    IF(J.EQ.9)Y(N)=0.0
33    CONTINUE
40    CONTINUE
50    CONTINUE
C
C-----------------------------------------------------------------
C
C               GENERATE ELEMENT CONNECTIVITY. THIS IS
C               DONE BY SETTING UP THE FIRST ELEMENT IN
C               EACH LAYER, AND REFERENCING THE REST
C               OF THE ELEMENTS IN THAT LAYER TO IT. THE
C               TASK IS SIMPLIFIED TO SOME EXTENT BECAUSE
C               ADINA HAS PROVISIONS FOR ELEMENT GENERATION.
C
C-----------------------------------------------------------------
C
      DO 99 I=1, LAYERS
      KEL(1,I)=(I-1)*16+1
      KG(1,I)=0
      NOD(1,1,I)=(I-1)*NN+1
      NOD(2,1,I)=NOD(1,1,I)+2
      NOD(3,1,I)=NOD(2,1,I)+NPR+NPRMID
      NOD(4,1,I)=NOD(3,1,I)-2
      DO 55 L=1,4
      NOD(L+4,1,I)=NOD(L,1,I)+NN
55    CONTINUE
      NOD(9,1,I)=NOD(1,1,I)+1
      NOD(10,1,I)=NOD(2,1,I)+NPR-1
      NOD(11,1,I)=NOD(9,1,I)+NPR+NPRMID
      NOD(12,1,I)=NOD(10,1,I)-1
      DO 56 L=1,4
      NOD(L+12,1,I)=NOD(L+8,1,I)+NN
56    CONTINUE
      KOUNT=1
      DO 57 J=2,NEL
      KCUNT=KOUNT+1
      KG(J,I)=0
                                    KEL(J,I)=KEL(J-1,I)+1
      NOD(1,J,I)=NOD(2,J-1,I)
      IF(KOUNT.EQ.(NDIV+2))NOD(1,J,I)=NOD(4,J-NDIV1,I)
      NOD(2,J,I)=NOD(1,J,I)+2
      NOD(3,J,I)=NOD(2,J,I)+NPR+NPRMID
      NOD(4,J,I)=NOD(3,J,I)-2
      DO 58 L=1,4
      NOD(L+4,J,I)=NOD(L,J,I)+NN
58    CONTINUE
      NOD(9,J,I)=NOD(1,J,I)+1
      NOD(10,J,I)=NOD(10,J-1,I)+1
      IF(KOUNT.EQ.(NDIV+2))NOD(10,J,I)=NOD(10,J-NDIV1,I)+NPR
      NOD(11,J,I)=NOD(3,J,I)-1                                 +NPRMID
      NOD(12,J,I)=NOD(10,J,I)-1
      DO 59 L=1,4
      NOD(12+L,J,I)=NOD(8+L,J,I)+NN
59    CONTINUE
      IF(KOUNT.EQ.(NDIV+2))KOUNT=1
      MAXEL=KEL(J,I)
57    CONTINUE
99    CONTINUE
C
C-----------------------------------------------------------------
C
C               DIRECT OUTPUT TC THE APPROPRIATE DEVICE.FOR
C               DATA CHECK FUNCTIONS THIS WOULD BE THE OFFLINE
C               PRINTER. WHEN THE DATA IS SATISFACTORY, OUTPUT
C               BE DIRECTED TO THE OFFLINE PUNCH. IT IS THEN RE
```

```
C             TO BE USED WITH THE ADINA JOB CONTROL DECK. TO
C             USE IT WITH PSAP1 SIMPLY REMOVE THE LOAD CARDS.
C
C-----------------------------------------------------------------
C
      WRITE(7,160)MAXEL,PTYPE
160   FORMAT(1X,I5,2X,'ELEMENT PLATE',15A4)
      WRITE(7,170)N,(IDOF(I),I=1,6),NEGL,NEGNL,MODEX,NSTE,
     *DT,TSTART,IPRI
170   FORMAT(I5,6I1,I4,3I5,2F10.0,I5)
      WRITE(7,180)
180   FORMAT(///)
      WRITE(7,190) NPB,IDC
190   FORMAT(16I5)
      WRITE(7,190)((IPNODE(I,J),I=1,2),J=1,NPB)
      DO 210 I=1,N
      WRITE(7,200) NODE(I),(ID(J,I),J=1,3),X(I),Y(I),Z(I)
200   FORMAT(1X,I4,1X,I4,2I5,15X,3E10.3)
210   CONTINUE
      WRITE(7,190)NLOAD,NLCUR,NPTM
      WRITE(7,190)ICON,IPRIC
      DO 220 I=1,20
      NPAR(I)=0
220   CONTINUE
      NPAR(1)=3
      NPAR(2)=MAXEL
      NPAR(3)=1
      NPAR(7)=16
      NPAR(10)=3
      NPAR(11)=3
      NPAR(15)=8
      NPAR(16)=1
      WRITE(7,230)(NPAR(I),I=1,20)
230   FORMAT(20I4)
      WRITE(7,190)MTYP
      WRITE(7,240) (PROP(I),I=1,4)
240   FORMAT(8E10.3)
      DO 270 I=1,LAYERS
      IPS=0
      IF(I.NE.1.OR.I.NE.LAYERS)IPS=1
      DO 260 J=1,NEL
      WRITE(7,250) KEL(J,I),IELD,IELX,IPS,MTYP,MAXES,IST,KG(J,I)
      WRITE(7,190)(NOD(K,J,I),K=1,8)
      WRITE(7,190)(NOD(K,J,I),K=9,16)
250   FORMAT(8I5,E10.3)
260   CONTINUE
270   CONTINUE
C
C-----------------------------------------------------------------
C
C             LOAD CARD GENERATION AND OUTPUT FOLLOWS
C
C
C-----------------------------------------------------------------
C
      DO 280 I=1,NSTE
      TIMV(I)=I-1
      RV(I)=PINC/80.0*FLOAT(I)
      IF(RV(I).GT.(PMAX/80.0))RV(I)=PMAX/80.0
      RV1(I)=RV(I)/2.0
280   CONTINUE
      WRITE(7,190)NTF1,NPTS
      WRITE(7,240)(TIMV(I),RV(I),I=1,NPTS)
      WRITE(7,190)NTF2,NPTS
      WRITE(7,240)(TIMV(I),RV1(I),I=1,NPTS)
      DO 300 I=1,9
      NCUR=1
      IF(I.EQ.1.OR.I.EQ.9) NCUR=2
      IF(MOD(I,2).EQ.0) GO TO 290
      NLD1=LAYERS*NN+1+(I-1)*(NPR+NPRMID)/2
      NLD2=NLD1+1
      NLD3=NLD2+1
      WRITE(7,310)NLD1,IDIRN,NCUR,FAC
```

```
      WRITE(7,310)NLD2,IDIRN,NCUR,FAC
      WRITE(7,310)NLD3,IDIRN,NCUR,FAC
      GO TO 300
290   NLD1=NLD1+NPR
      NLD2=NLD1+1
      WRITE(7,310)NLD1,IDIRN,NCUR,FAC
      WRITE(7,310)NLD2,IDIRN,NCUR,FAC
300   CONTINUE
310   FORMAT(3I5,F10.0)
      STOP
      END
```

$E_{11} = 21.0 \times 10^6$ psi

$E_{22} = 1.7 \times 10^6$ psi

$G_{12} = .65 \times 10^6$ psi

$\nu_{12} = .21$

$\nu_{21} = .017$

| | 8-ply spar | 8-ply rib | 16-ply rib |
|---|---|---|---|
| $D_{11}$ | 169.3 | 634.4 | 4815 |
| $D_{12}$ | 99.7 | 89.7 | 914.1 |
| $D_{22}$ | 634.4 | 169.3 | 1379 |
| $D_{66}$ | 112.1 | 112.1 | 1014 |
| $D_{16}$ | 0 | 0 | 0 |
| $D_{26}$ | 0 | 0 | 0 |

High Strength Graphite-Epoxy material properties

TABLE I

MATERIAL

| | 2024T3 | 6061T6 | 7075T6 |
|---|---|---|---|
| t(ins) | 0.25 | .080 | .050 |
| a(ins) | 4.0 | 4.0 | 4.0 |
| Theoretical Mo,(in-lb) Py,(lb.) | 3520. | 272. | 175. |
| Experimental $M_f$,$P_f$ (in.lb.)(lb.) | 4800. | 380. | 246. |
| Theoretical (plate) Mo, $P_y$ | 4928. | 310. | 240. |

TABLE II

| Plate# | Specimen# | a | Pull Load at failure, $P_f$ | Moment at failure, $M_f(Pa/4)$ | Mult | Pult | Remarks |
|---|---|---|---|---|---|---|---|
| 2 | 15 | - | 1115 | -- | -- | 1115 | Pull through to determine Pult. crack noted at a load of 650. |
| 3 | 15A | - | 1160 | -- | -- | 1160 | Repeat of 15. Fastener noted at load of 525. |
| 4 | 71 | - | 2925 | -- | -- | 2925 | 16-ply plate. cracking first noted at load of 1100. |
| 5 | 27 | - | 1135 | -- | -- | 1135 | Repeat of 15 and 15A. cracking noted at load of 540. |
| 1 | 53 | 2 | 530 | 265 | 265 | -- | Line load at center span (beam) spar specimen. No cracking until failure. |
| 2 | 66 | 2 | 1235 | 617.5 | 617.5 | -- | Line load at center span (beam)8-ply rib specimen. No cracking until failure. |
| 3 | 11 | 2 | 1160 | 580 | 580 | -- | Repeat on specimen 66. |
| 4 | 76 | 4 | 1750 | 1750 | 1750 | -- | Line load at center span, 16-ply rib specimen, no cracking until failure. |
| 5 | 26 | 2 | 1110 | 555 | 555 | -- | Repeat of 66 and 11. |
| 1 | 52 | 2 | 452 | 226 | 265 | 1135 | 8-ply spar specimen failed across entire width. |
| 2 | 6 | 2 | 457 | 228.5 | 265 | 1115 | Repeat of 52. Failed across entire width. Started cracking at 420. |
| 2 | 7 | 4 | 255 | 255 | 265 | 1115 | 8-ply spar specimen failed across entire width, no cracking noted prior to failure. |
| 2 | 4 | 2 | 660 | 330 | 617.5 | 1115 | 8-ply rib specimen. Entire section did not fail (about 20% left intact) cracking noted at 520. |

TABLE III.

| Plate# | Specimen# | a | Pull Load at failure, $P_f$ | Moment at failure, $M_f(Pa/4)$ | Mult | Pult | Remarks |
|---|---|---|---|---|---|---|---|
| 3 | 64 | 4 | 410 | 410 | 500 | 1160 | 8-ply rib specimen pull through failure. Cracking first noted at load of 415. |
| 3 | 9 | 5 | 330 | 412.5 | 580 | 1160 | 8-ply rib specimen. No cracking prior to failure. Failure across entire width. |
| 3 | 10 | 3 | 603 | 452.25 | 580 | 1160 | 8-ply rib specimen. pull through failure. no cracking noted prior to failure. |
| 4 | 75 | 6 | 985 | 1477.5 | 1750 | 2925 | 16-ply rib specimen. Crack noted at load of 750. Failed across entire width. |
| 4 | 74 | 5 | 1085 | 1356.25 | 1750 | 2925 | 16-ply rib specimen. pull through failure. cracking noted at load of 865. |
| 4 | 13 | 4 | 1075 | 1075 | 1750 | 2925 | 16-ply rib specimen. pull through failure. cracking noted at load of 785. |
| 4 | 73 | 4 | 1140 | 1140 | 1750 | 2925 | Repeat of 13. |
| 4 | 72 | 3 | 1255 | 941.25 | 1750 | 2925 | 16-ply rib specimen. pull through failure. cracking noted at load of 1050. |
| 5 | 65 | 5 | 302 | 377.5 | 555 | 1135 | Repeat of 9. cracking noted at load of 140.failure across entire width. |
| 5 | 21 | 4 | 365 | 365 | 555 | 1135 | 8-ply rib specimen. repeat of 8, no cracking until failure across entire width. |
| 5 | 63 | 3 | 582 | 4365 | 555 | 1135 | 8-ply rib specimen, repeat of 10. cracking noted at 225. pull through failure. |
| 5 | 62 | 2 | 605 | 302.5 | 555 | 1135 | 8-ply rib specimen. repeat of 4. pull through failure. cracking at 457. |

TABLE III (Continued)

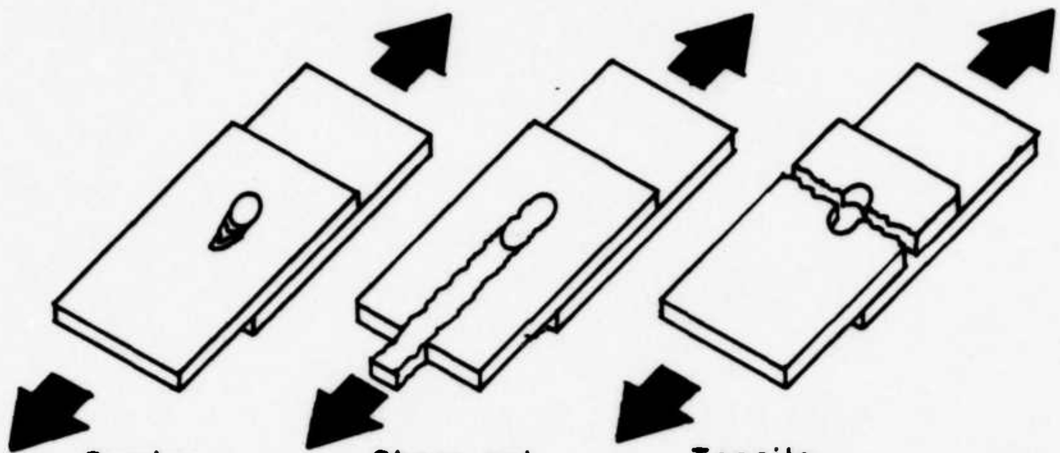


Figure 1

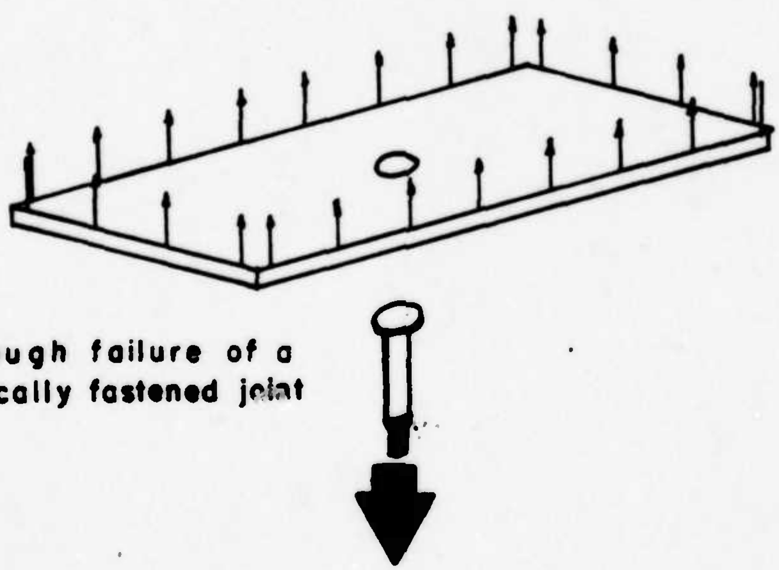


Figure 2

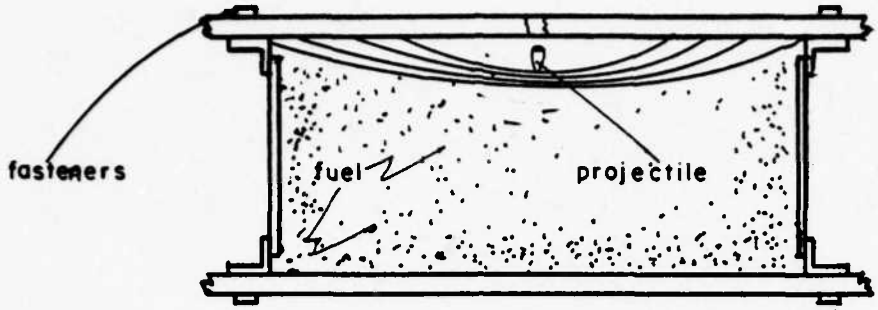


**Phase I**

Propagation of shock through fluid

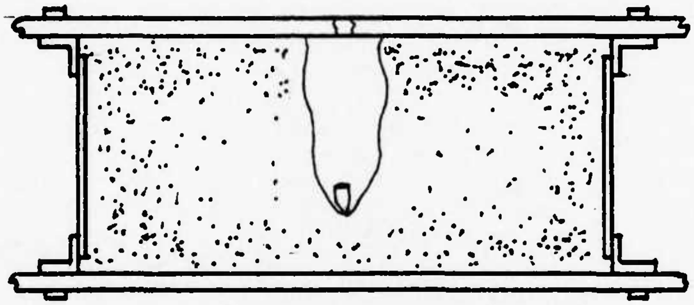

**Phase II**

Formation of vapor filled cavity

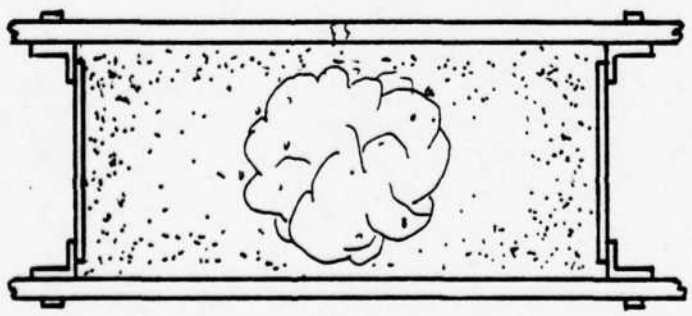

**Phase III**

Oscillation of cavity

**Figure 3**

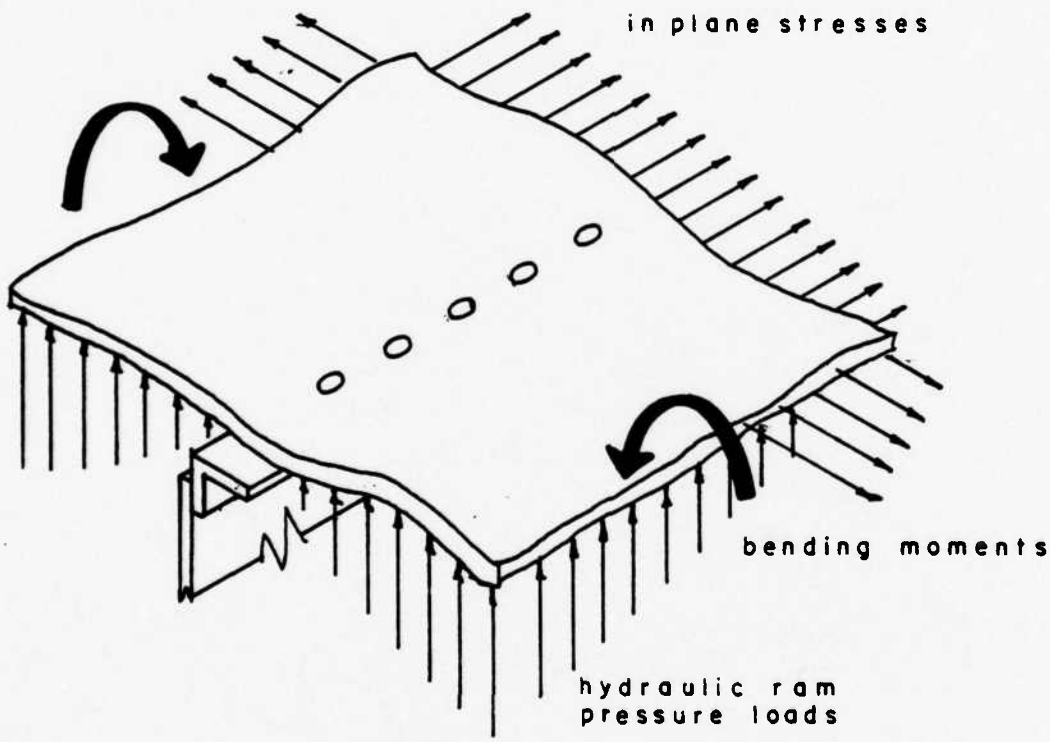


Pressure, stress and moment
distribution induced by
hydraulic ram

Figure 4

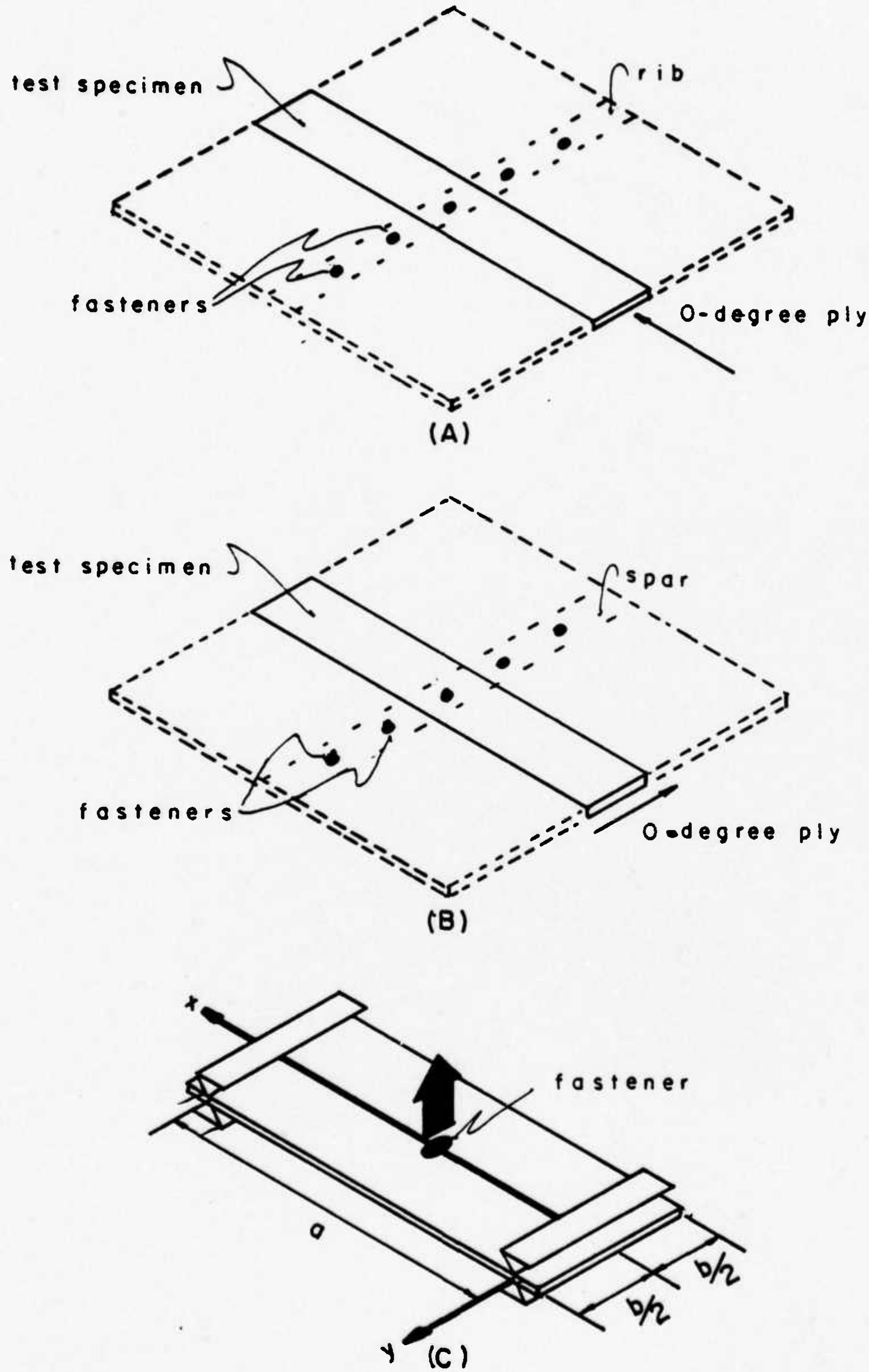


The model

Figure 5

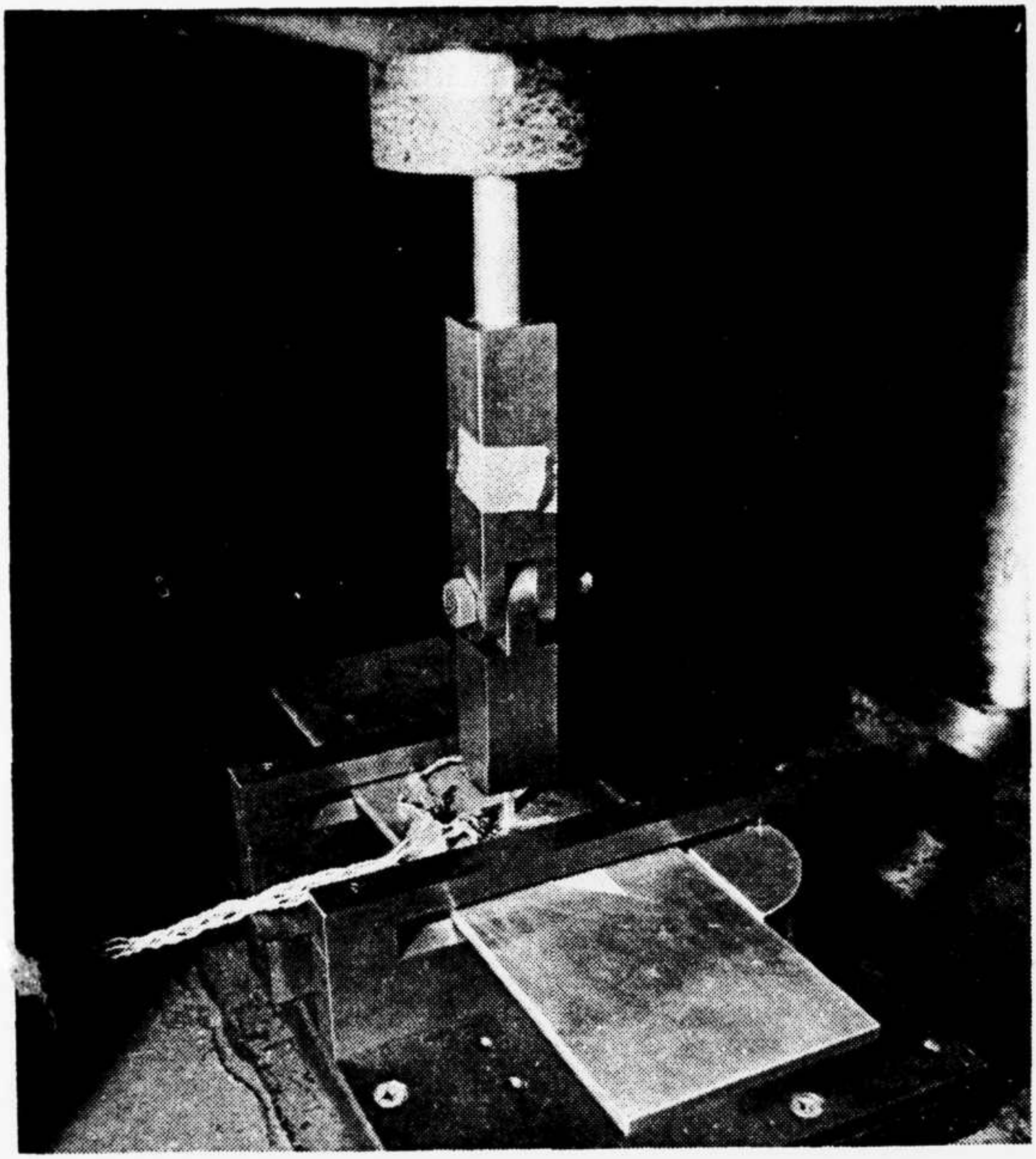

Simple support device with aluminum specimen in place

Figure 6

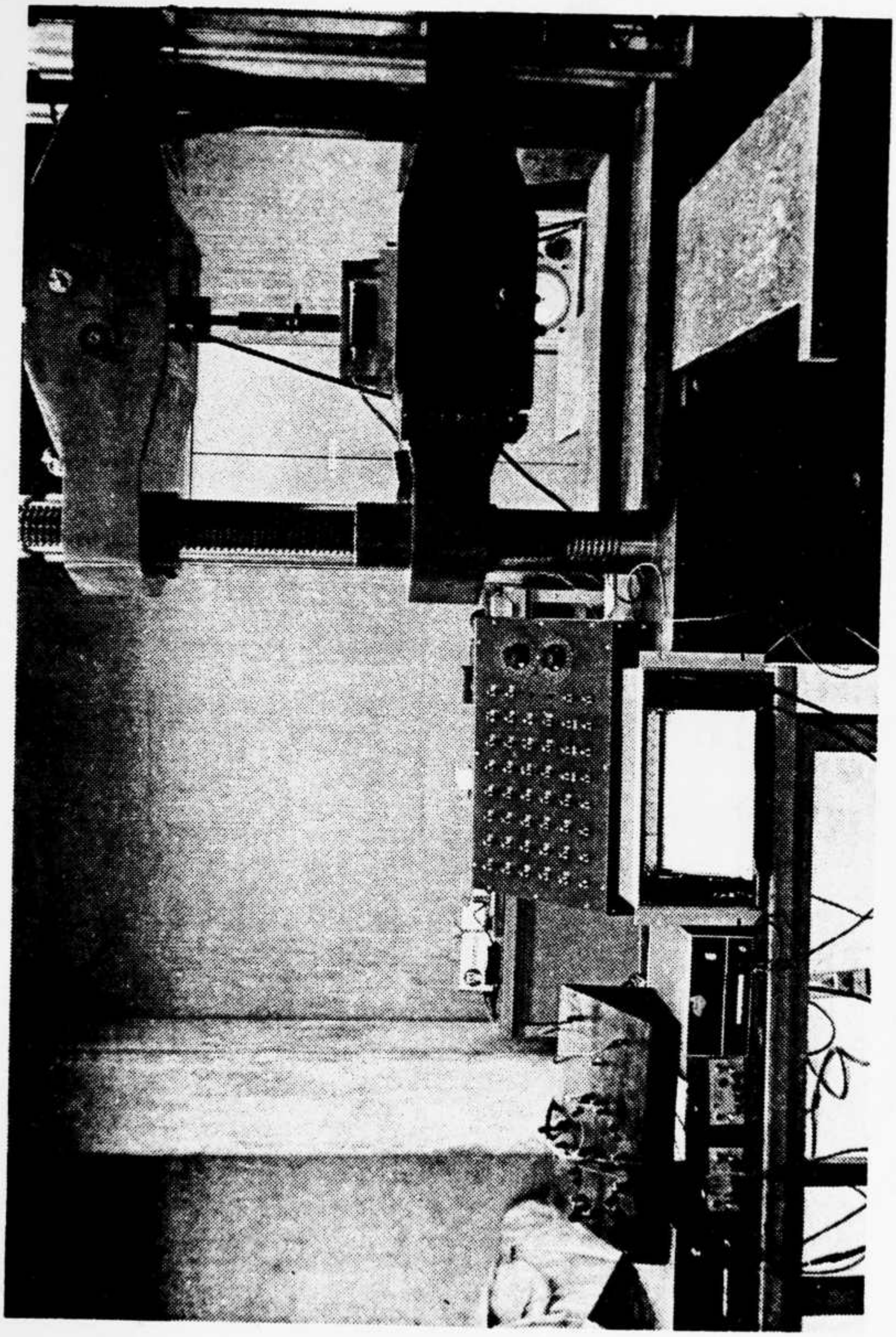

Experimental facility

Figure 7

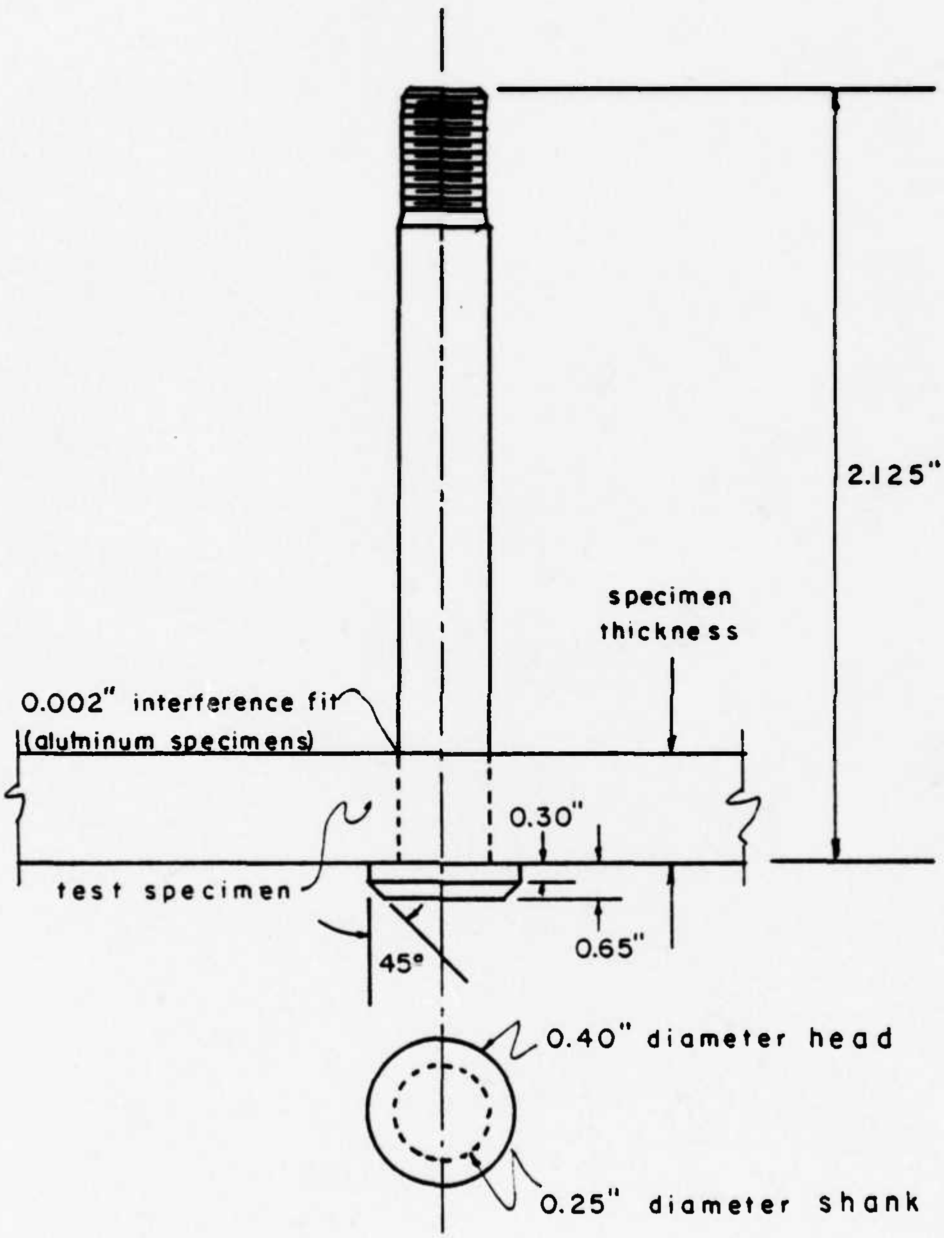


HL 328-8-18 fastener used in the tests
(Patent held by Hi-Shear corp.)

Figure 8

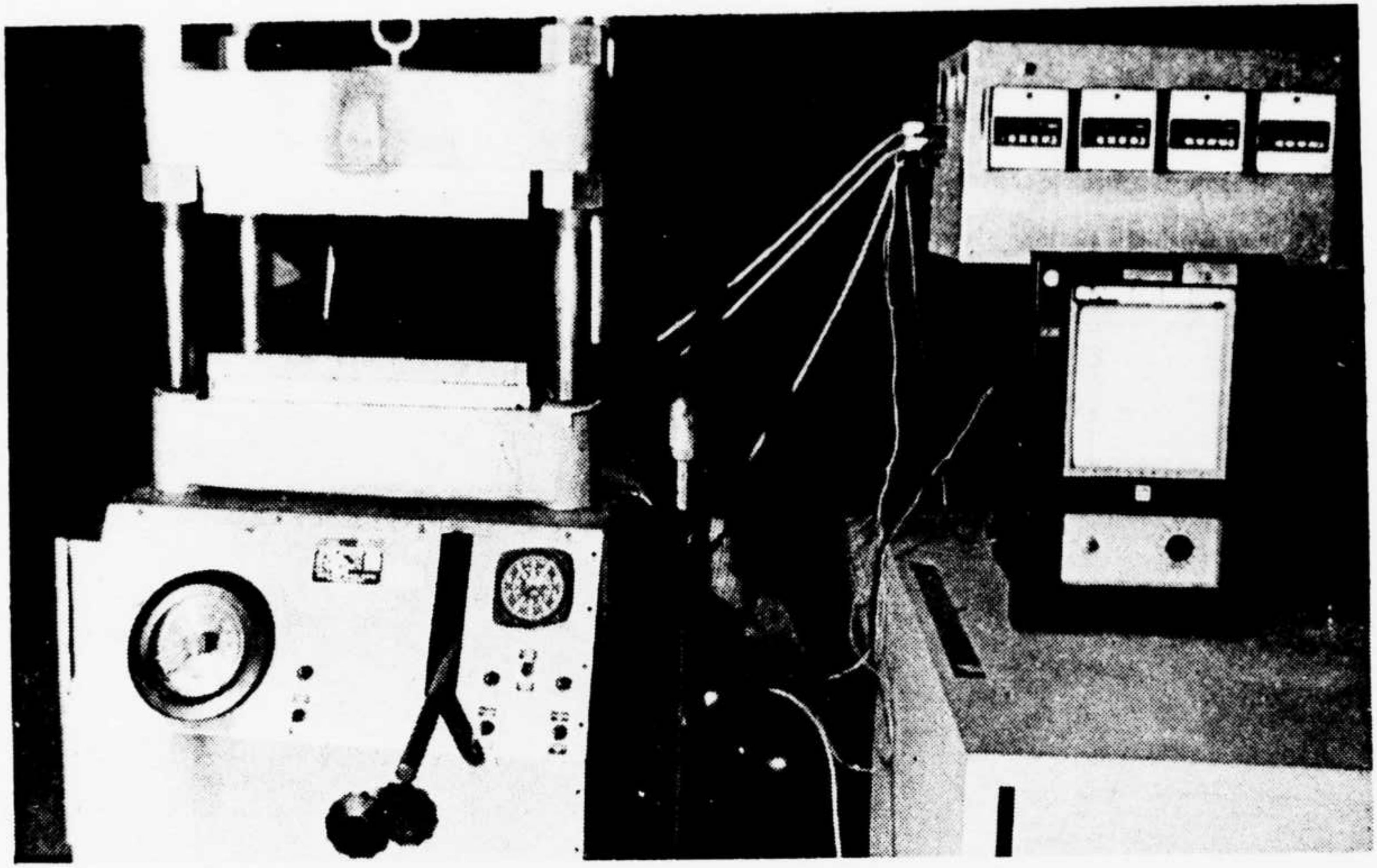

Composite preparation equipment

Figure 9

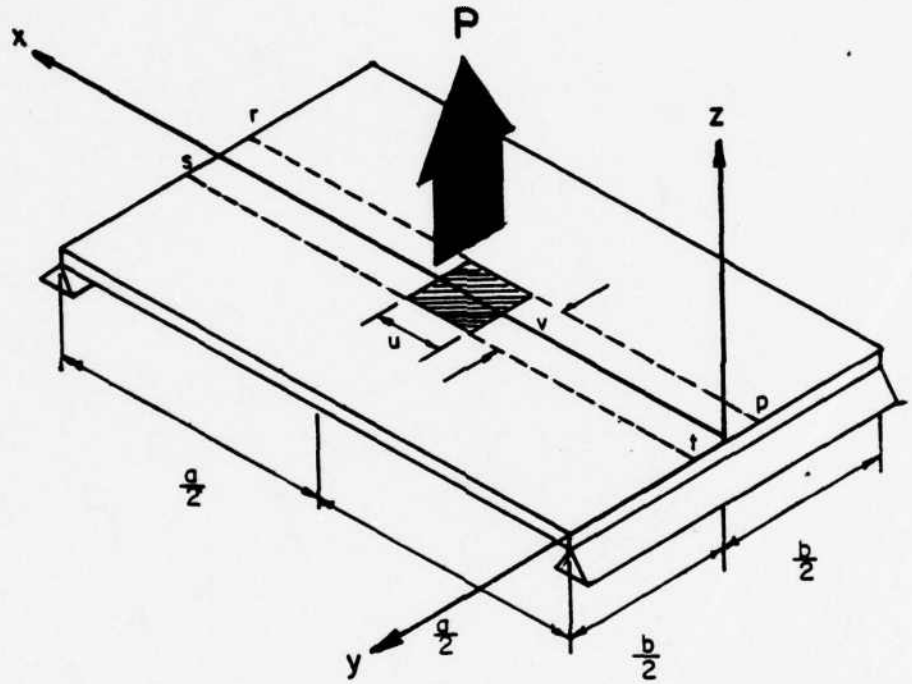


Test-specimen idealization

Figure 10

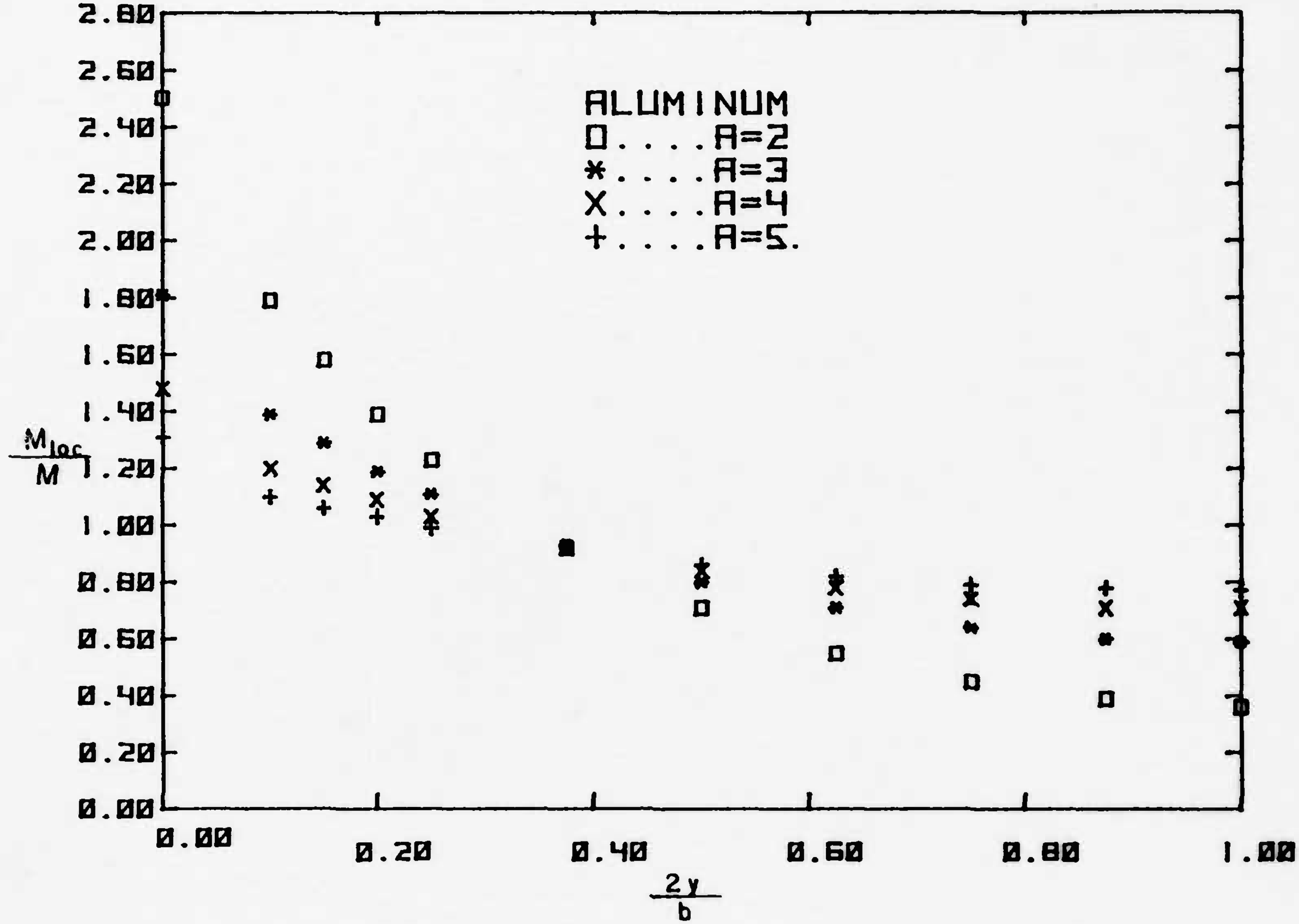
ALUMINUM
□....A=2
*....A=3
X....A=4
+....A=5.
2.80
2.60
2.40
2.20
2.00
1.80
1.60
1.40
1.20
1.00
0.80
0.60
0.40
0.20
0.00
$\frac{M_{loc}}{M}$
0.00
0.20
0.40
0.60
0.80
1.00
$\frac{2y}{b}$

Figure 11A

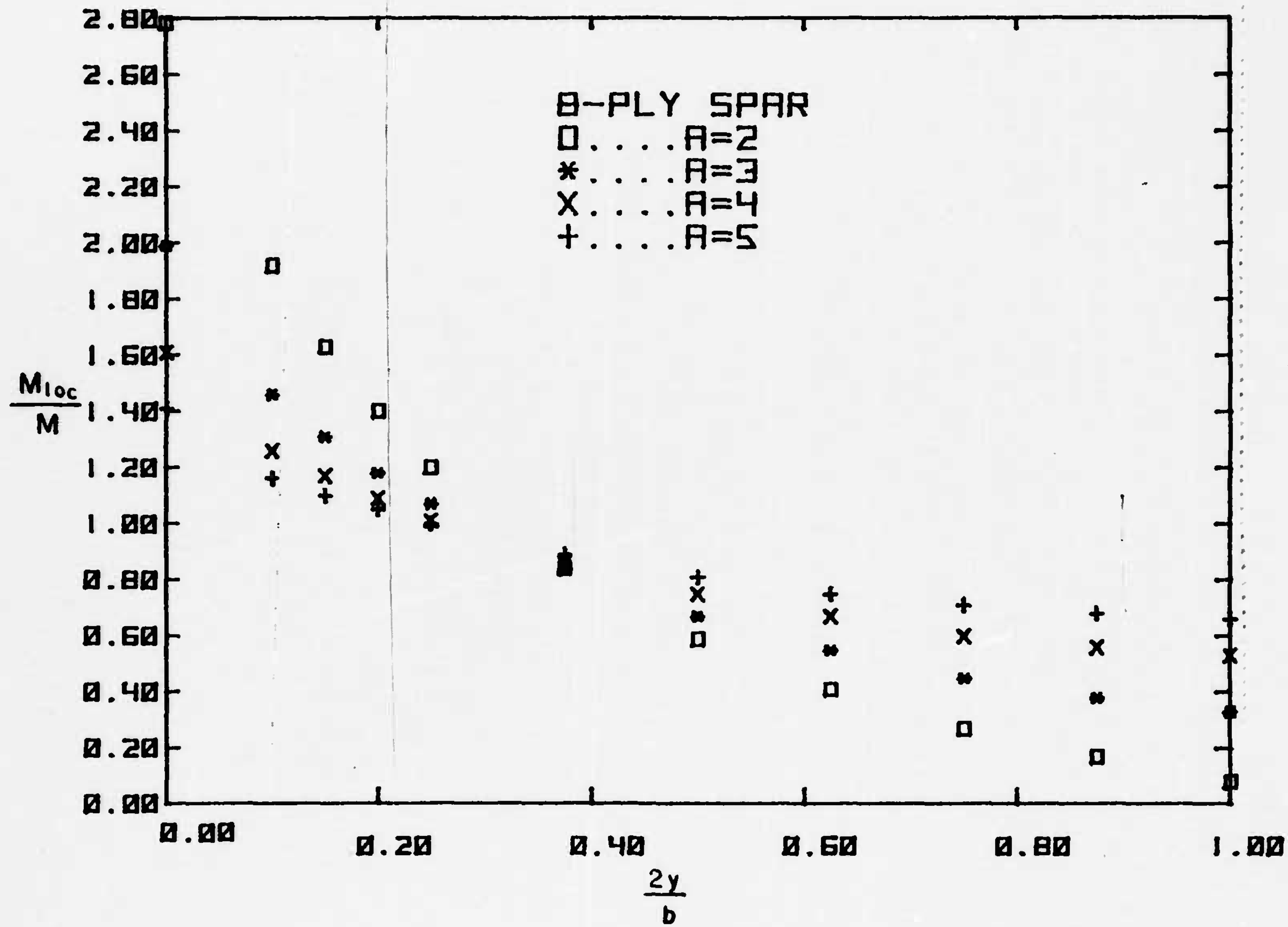
8-PLY SPAR
□....A=2
*....A=3
X....A=4
+....A=5
2.80
2.60
2.40
2.20
2.00
1.80
1.60
1.40
1.20
1.00
0.80
0.60
0.40
0.20
0.00
0.00
0.20
0.40
0.60
0.80
1.00
$\frac{M_{loc}}{M}$
$\frac{2y}{b}$

Figure 11B

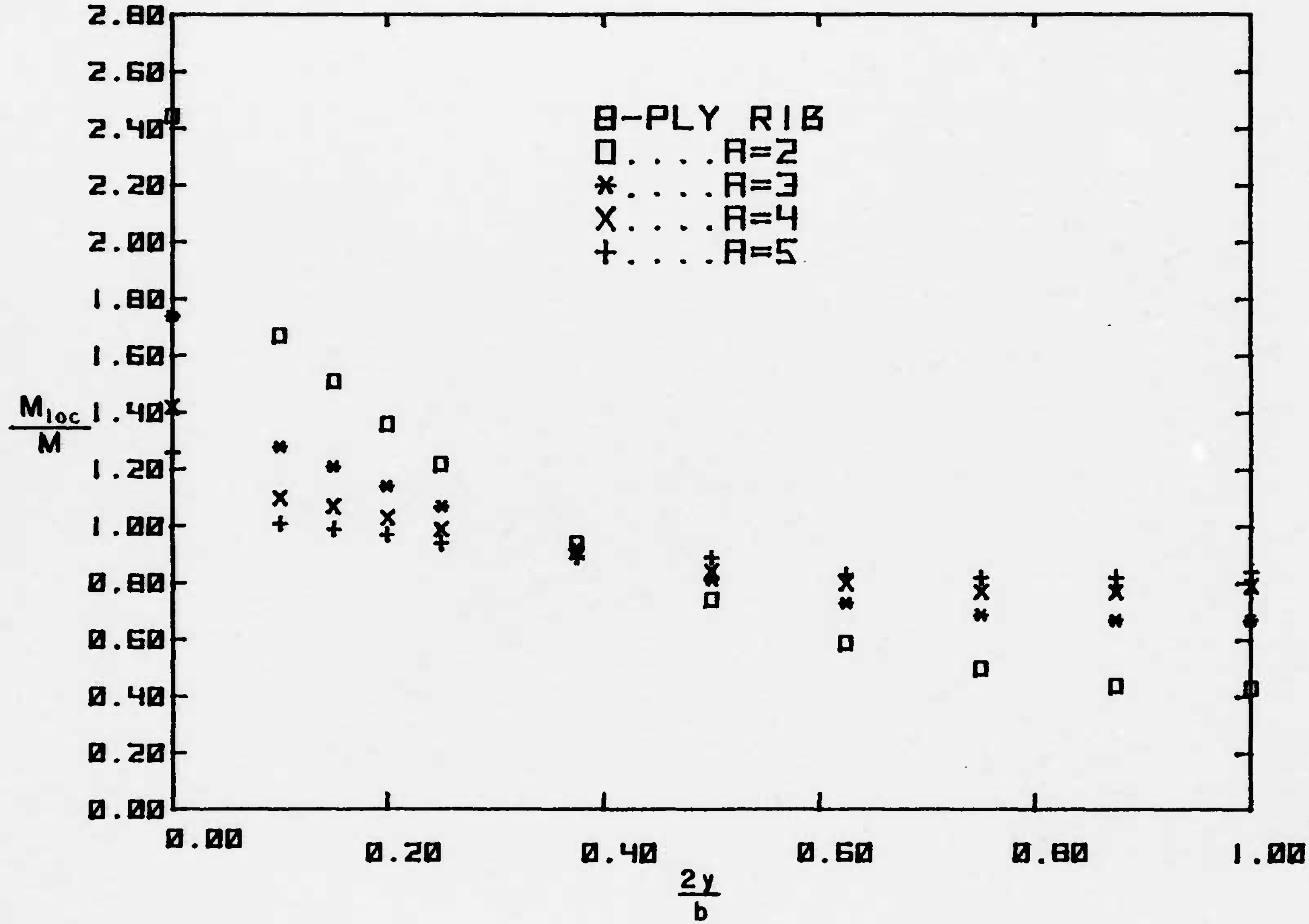
8-PLY RIB
□....A=2
*....A=3
X....A=4
+....A=5
2.80
2.60
2.40
2.20
2.00
1.80
1.60
1.40
1.20
1.00
0.80
0.60
0.40
0.20
0.00
0.20
0.40
0.60
0.80
1.00
$\frac{M_{loc}}{M}$
$\frac{2y}{b}$

Figure 11C

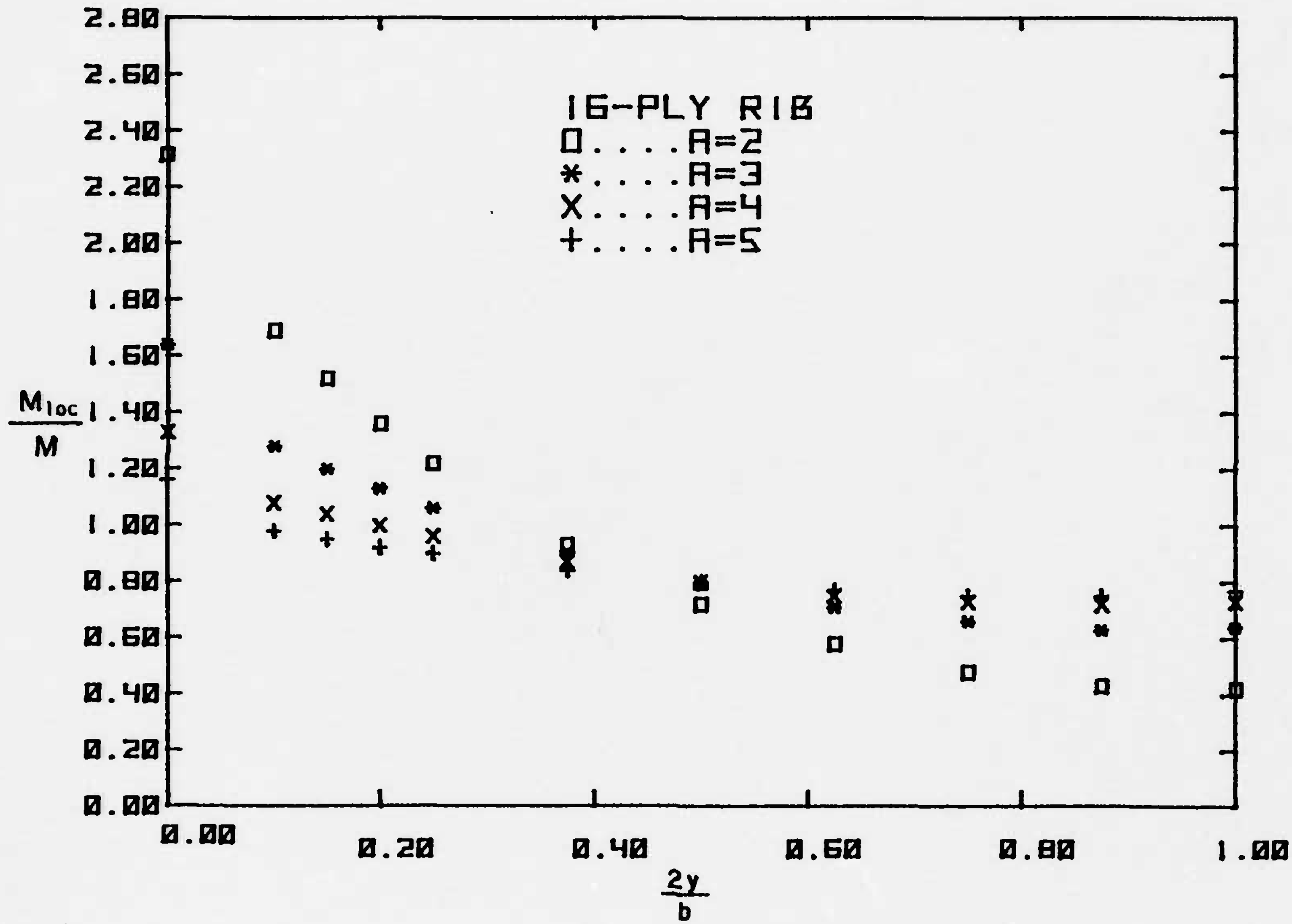
16-PLY RIB
□....A=2
*....A=3
X....A=4
+....A=5
$\frac{M_{loc}}{M}$
$\frac{2y}{b}$
2.80
2.60
2.40
2.20
2.00
1.80
1.60
1.40
1.20
1.00
0.80
0.60
0.40
0.20
0.00
0.20
0.40
0.60
0.80
1.00

Figure 11D

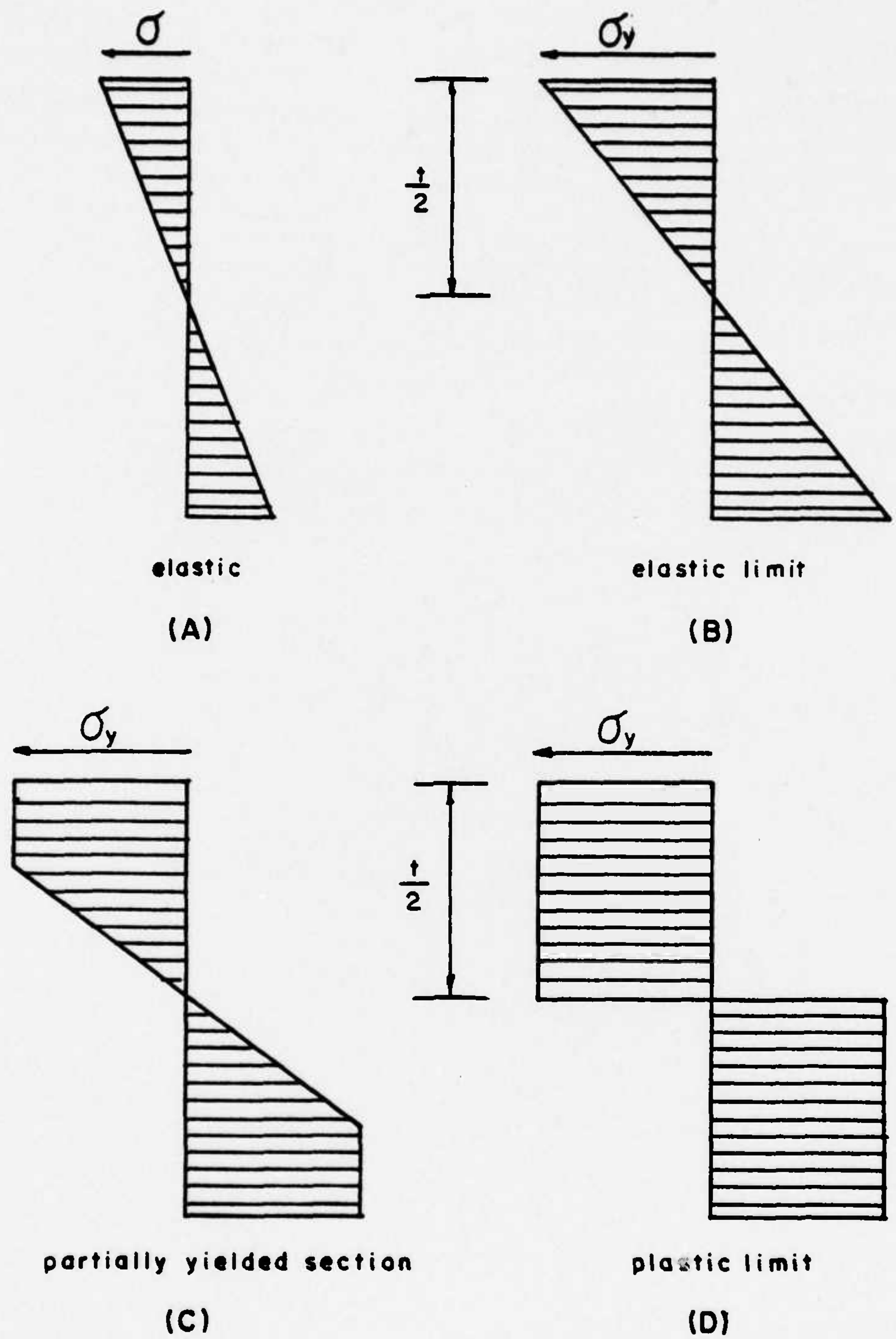


Stress distribution in a rectangular beam

Figure 12

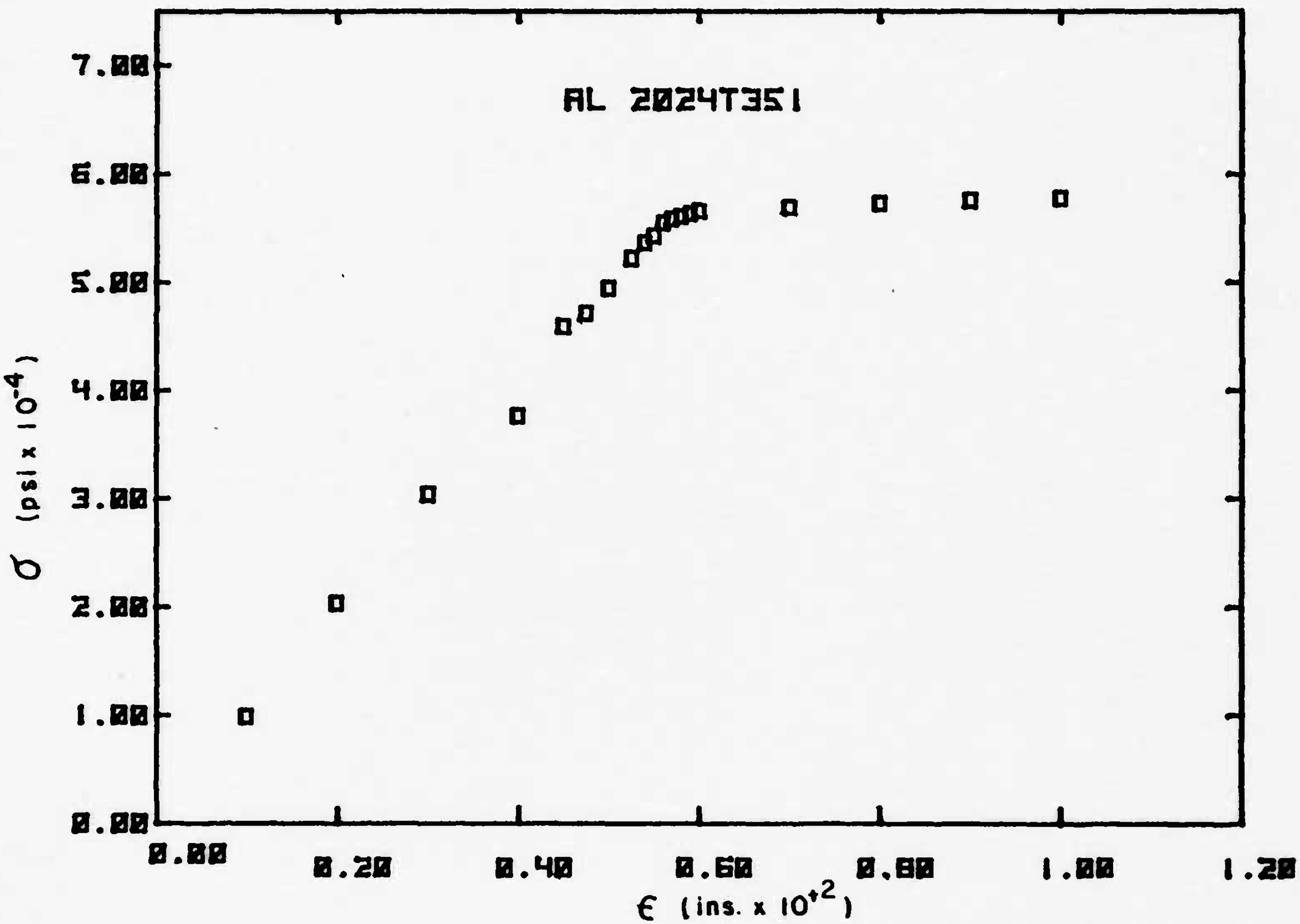
AL 2024T351
7.00
6.00
5.00
4.00
3.00
2.00
1.00
0.00
σ (psi x 10-4)
0.00
0.20
0.40
0.60
0.80
1.00
1.20
ϵ (ins. x 10+2)

Figure 13A

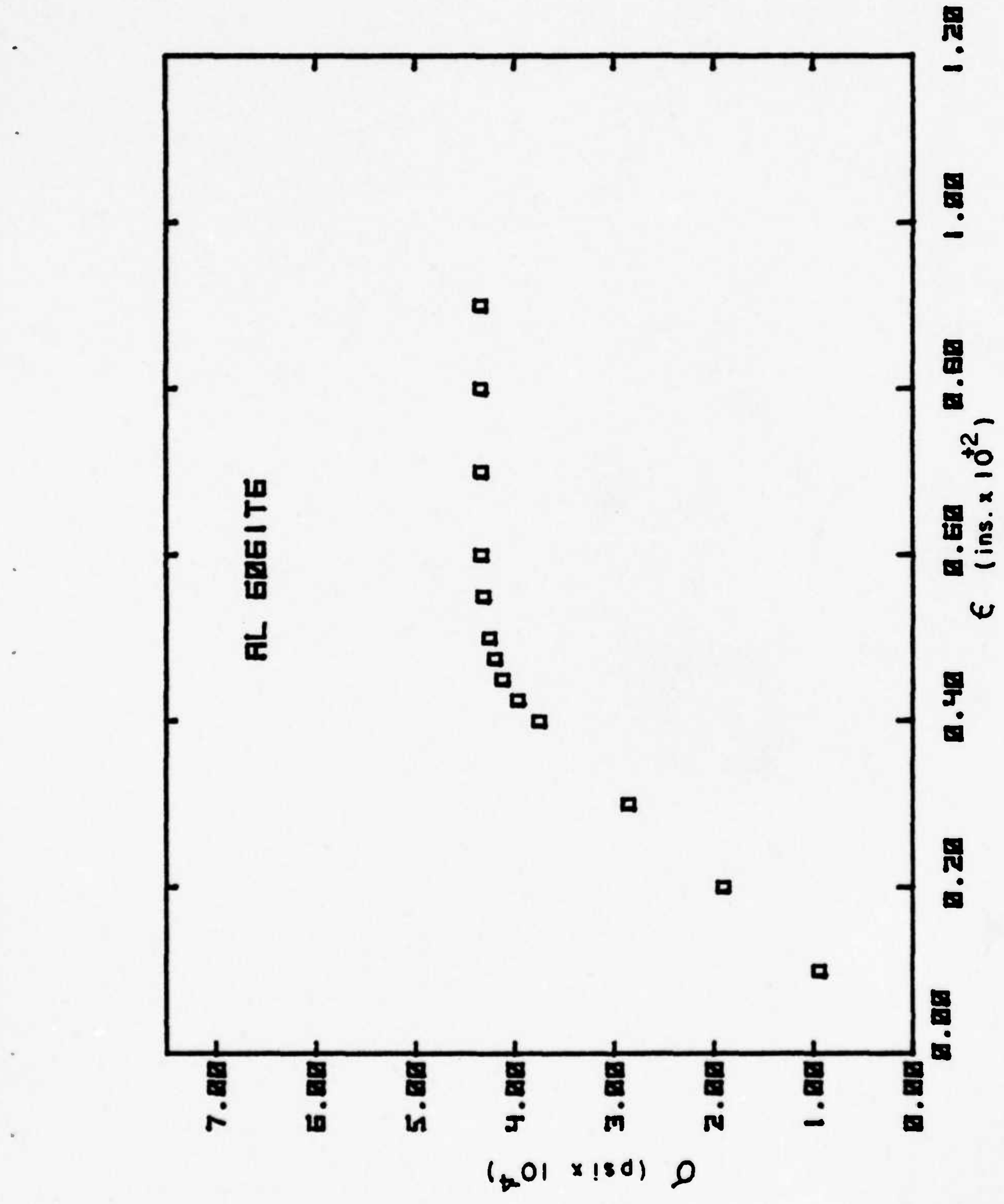
AL 6061T6
7.00
6.00
5.00
4.00
3.00
2.00
1.00
0.00
σ (psi x 10⁴)
0.00
0.20
0.40
0.60
0.80
1.00
1.20
ε (ins. x 10²)

Figure 13B

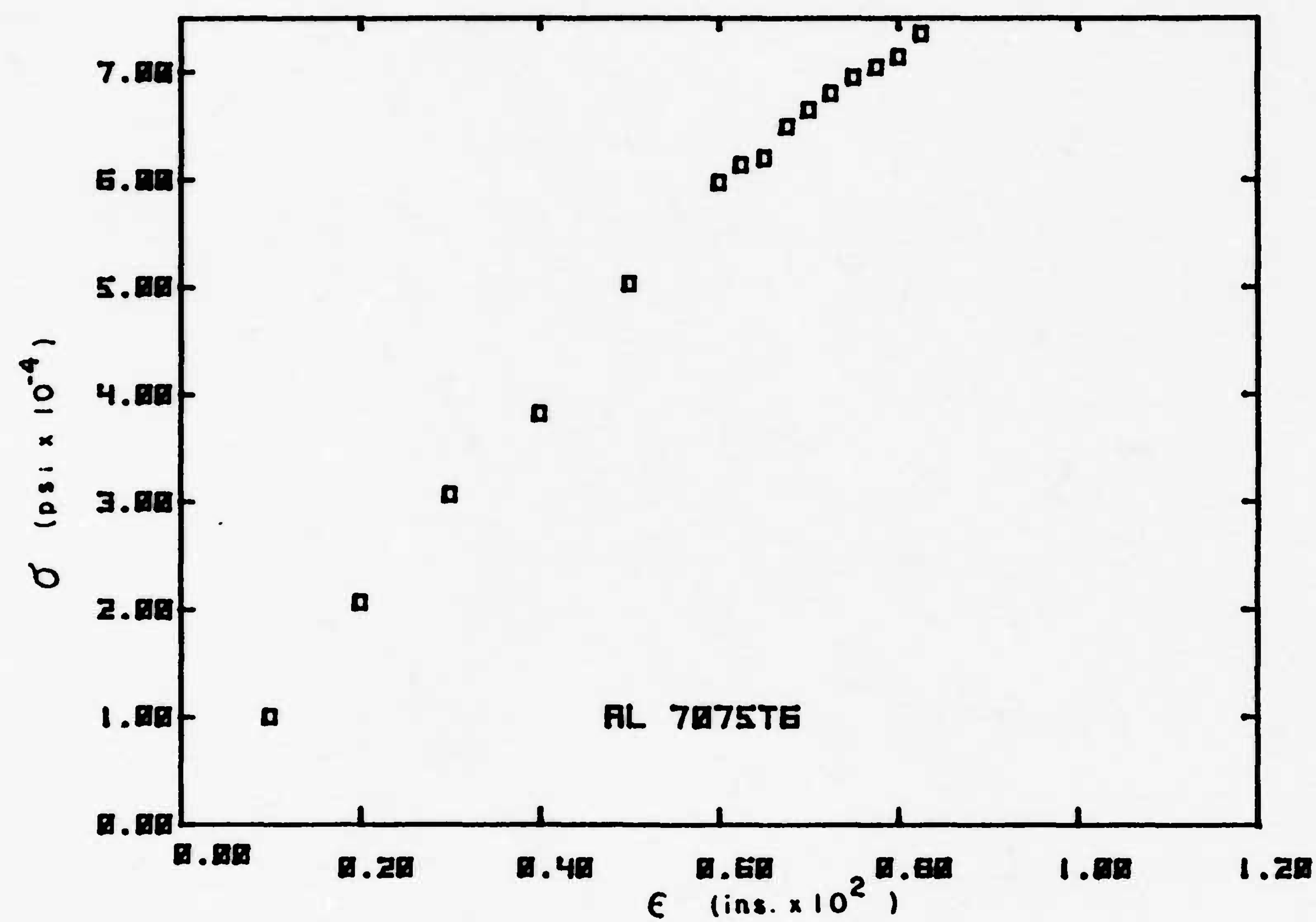
7.00
6.00
5.00
4.00
3.00
2.00
1.00
0.00
σ (psi x 10-4)
0.00
0.20
0.40
0.60
0.80
1.00
1.20
ε (ins. x 10^2 )
AL 7075T6

Figure 13C

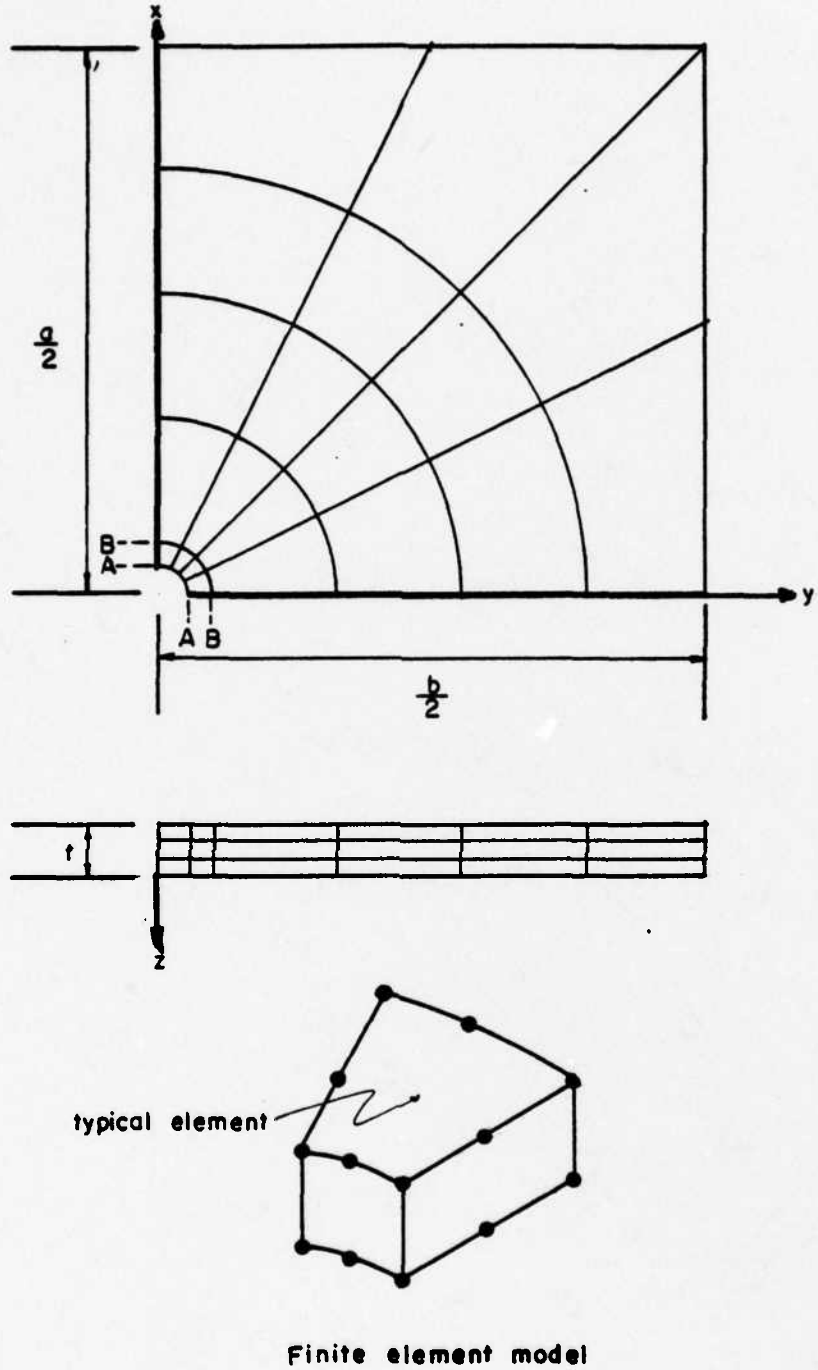


Figure 14

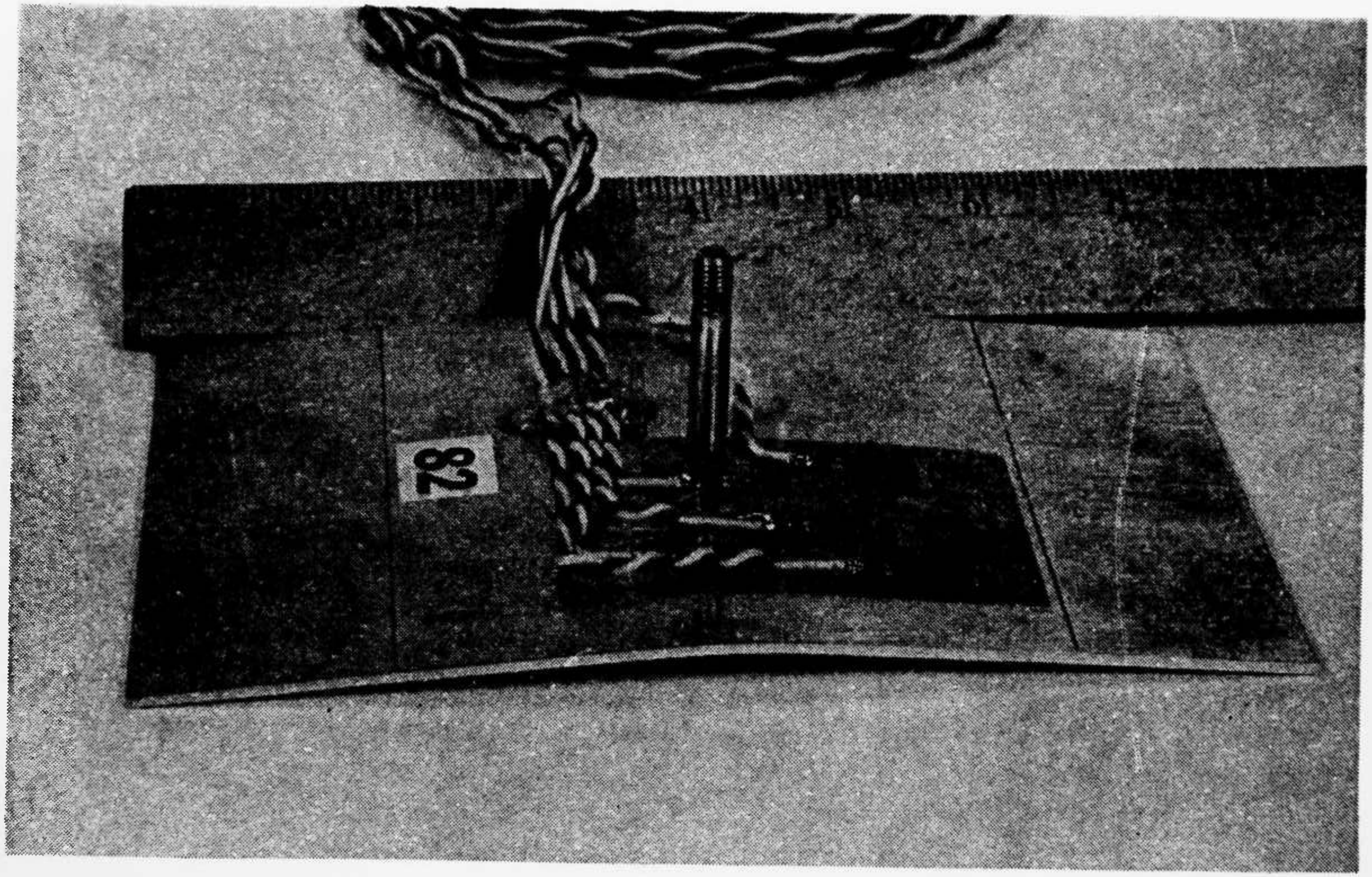


Aluminum specimen

Figure 15

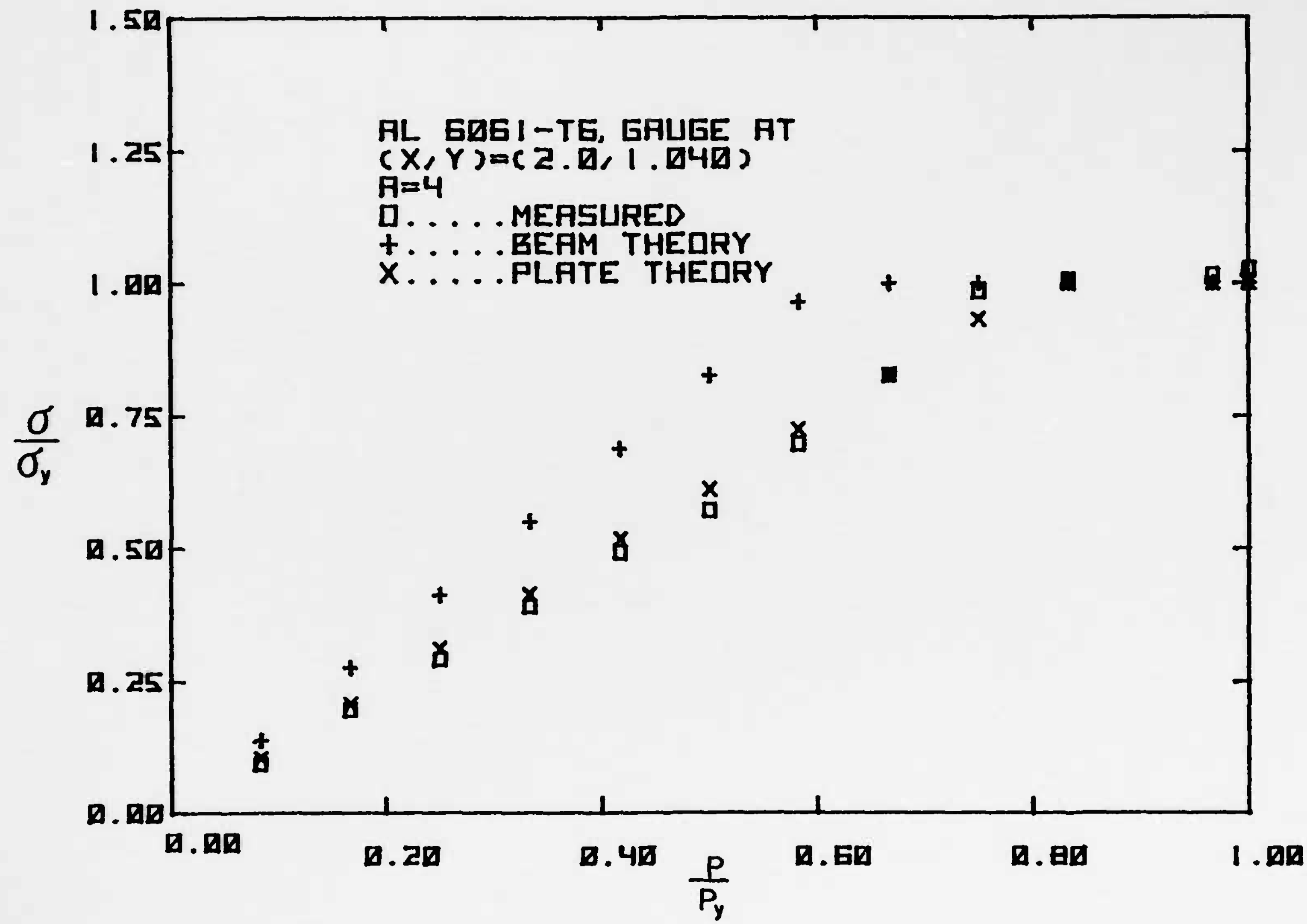
AL 6061-T6, GAUGE AT
(X,Y)=(2.0,1.040)
A=4
□.....MEASURED
+.....BEAM THEORY
X.....PLATE THEORY
1.50
1.25
1.00
0.75
0.50
0.25
0.00
0.00
0.20
0.40
0.60
0.80
1.00
$\frac{\sigma}{\sigma_y}$
$\frac{P}{P_y}$

Figure 16

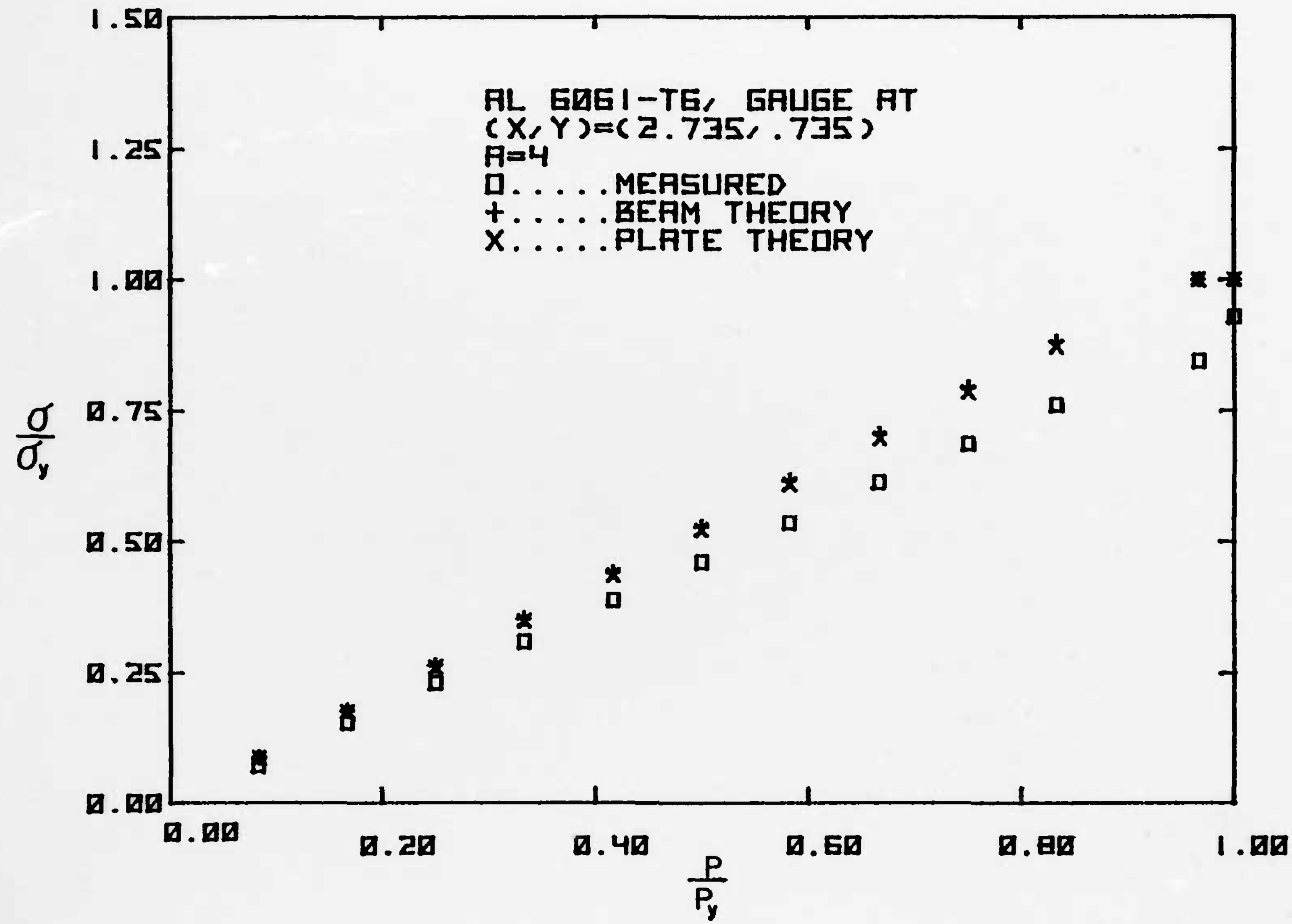

AL 6061-T6, GAUGE AT
(X,Y)=(2.735,.735)
A=4
□.....MEASURED
+.....BEAM THEORY
X.....PLATE THEORY
1.50
1.25
1.00
0.75
0.50
0.25
0.00
0.00
0.20
0.40
0.60
0.80
1.00


Figure 17

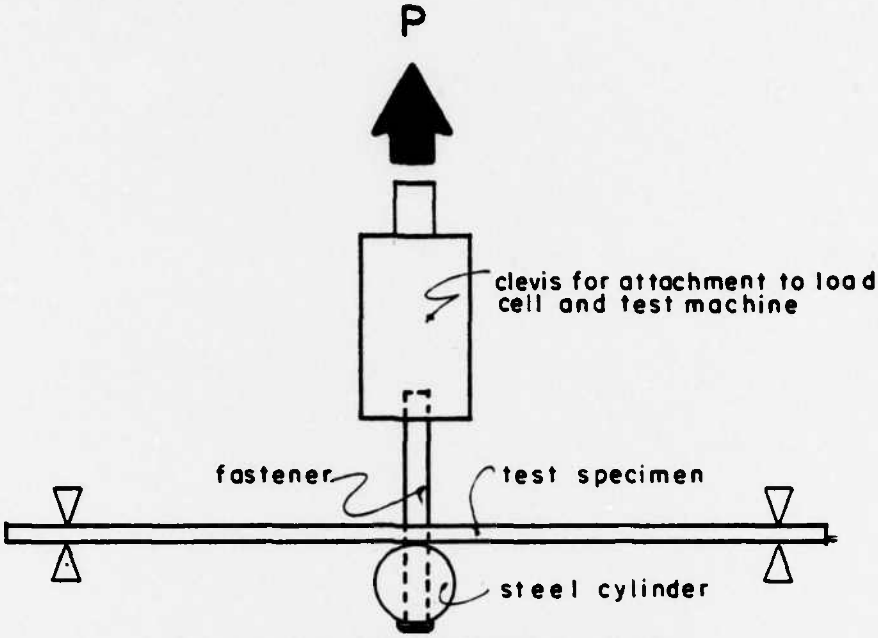


Set up for determination of $M_{ult}$

(A)

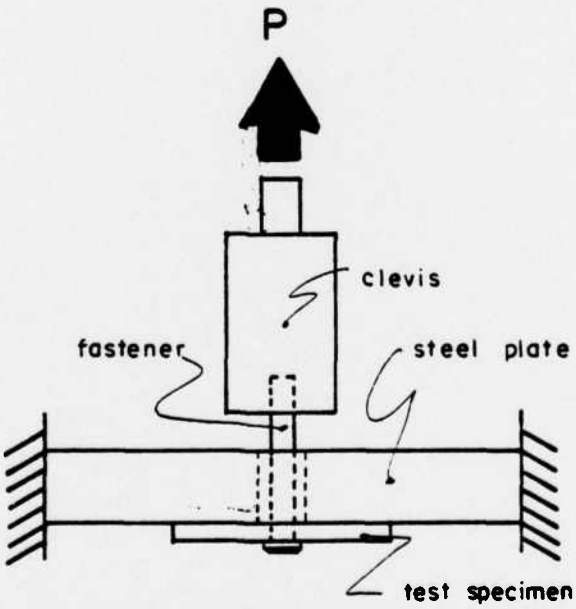


Set up for determination of $P_{ult}$

(B)

Figure 18

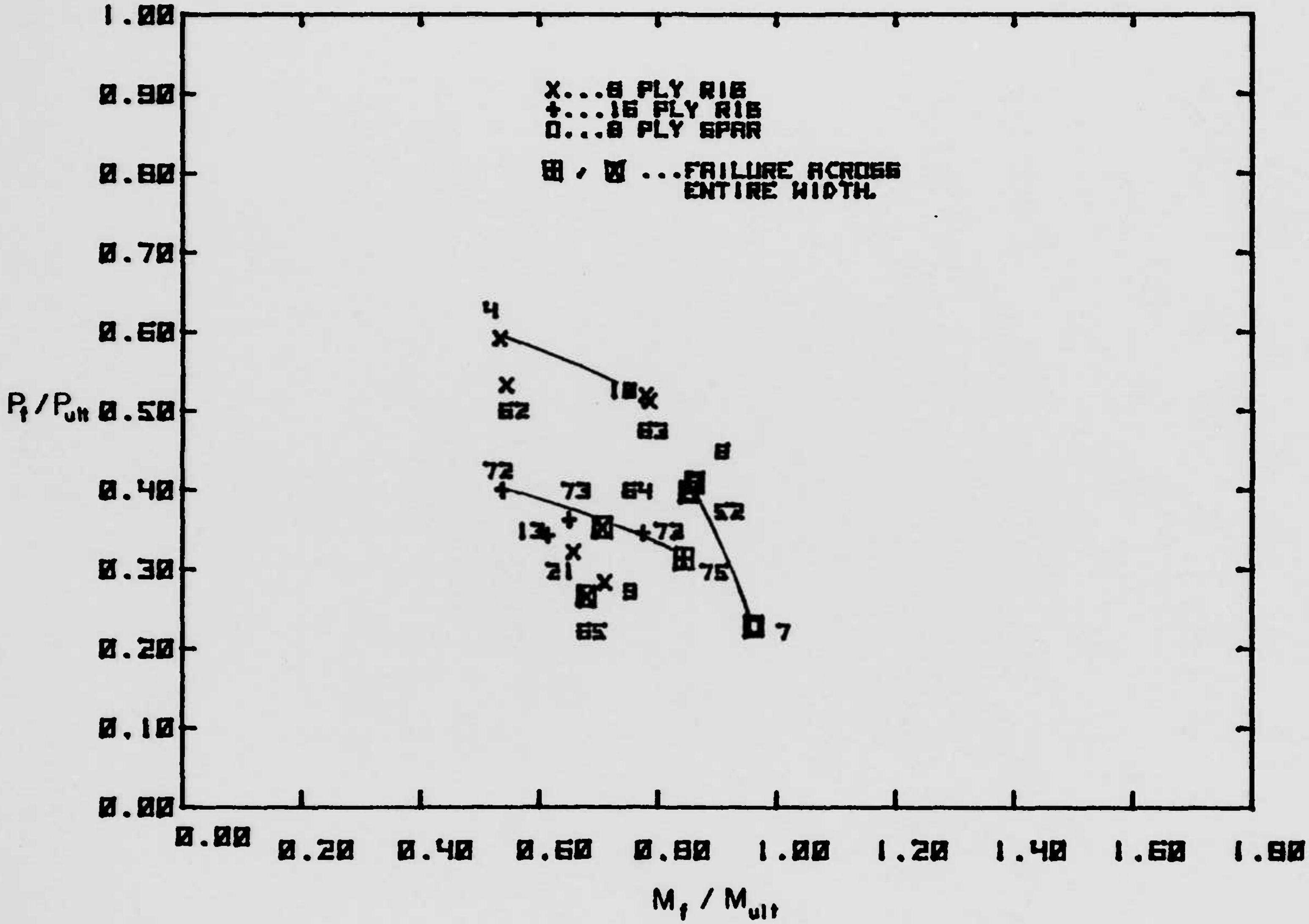
X...8 PLY RIB
+...16 PLY RIB
□...8 PLY SPAR
⊞ , ⊠ ...FAILURE ACROSS ENTIRE WIDTH.
1.00
0.90
0.80
0.70
0.60
0.50
0.40
0.30
0.20
0.10
0.00
0.20
0.40
0.60
0.80
1.00
1.20
1.40
1.60
1.80
4
62
18
63
8
72
73
64
52
13
73
21
75
9
65
7
$P_f / P_{ult}$
$M_f / M_{ult}$

Figure 19

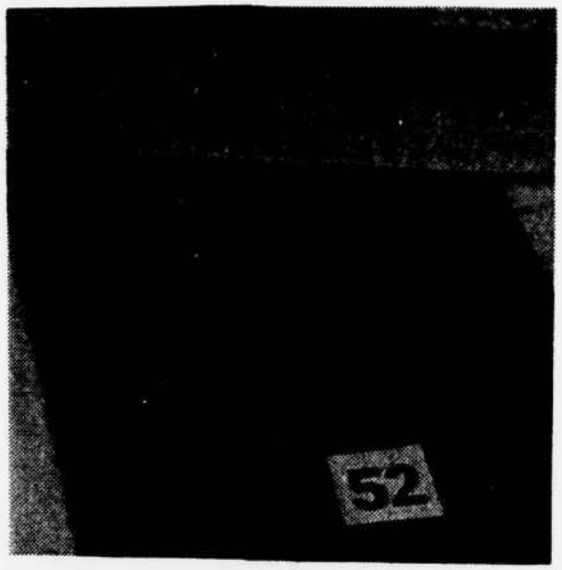


(A) $a = 2''$, spar specimen
$P_f = 452$ lbs.


(B) $a = 2''$, spar specimen,
line load, $P_f = 530$ lbs.

Figure 20


(C) through-plane shear, small moment, 8-ply, $P_f$ = 1135 lbs.

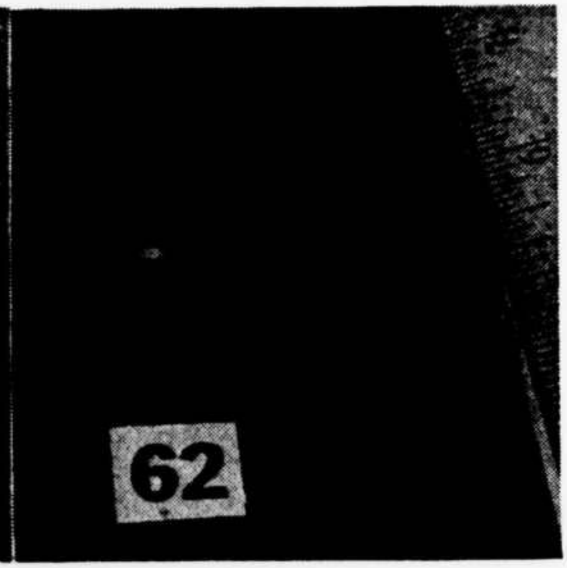


(D) a = 2", 8-ply rib specimen, $P_f$ = 605 lbs.

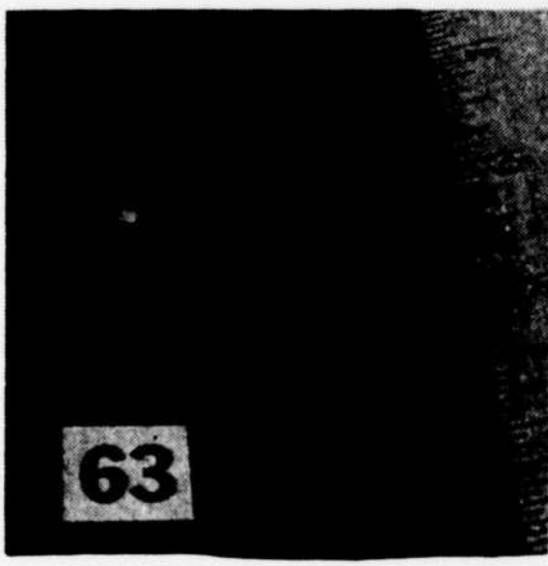


(E) a = 3", 8-ply rib specimen, $P_f$ = 582 lbs.

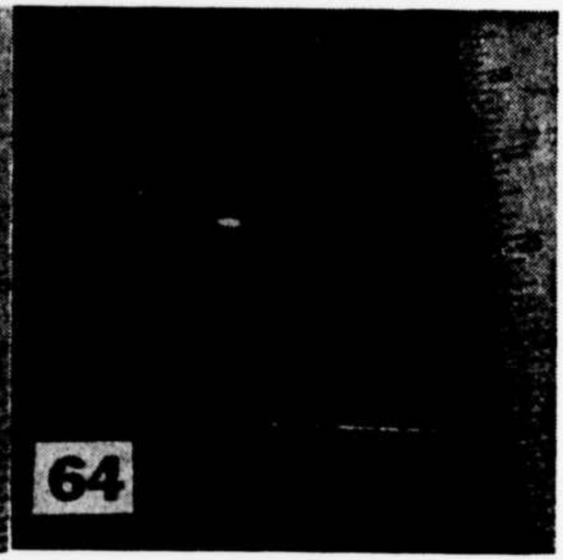


(F) a = 4", 8-ply rib specimen, $P_f$ = 410 lbs.

Figure 20 (cont'd)


(G) a=5", 8-ply rib specimen, $P_f$ = 302 lbs.

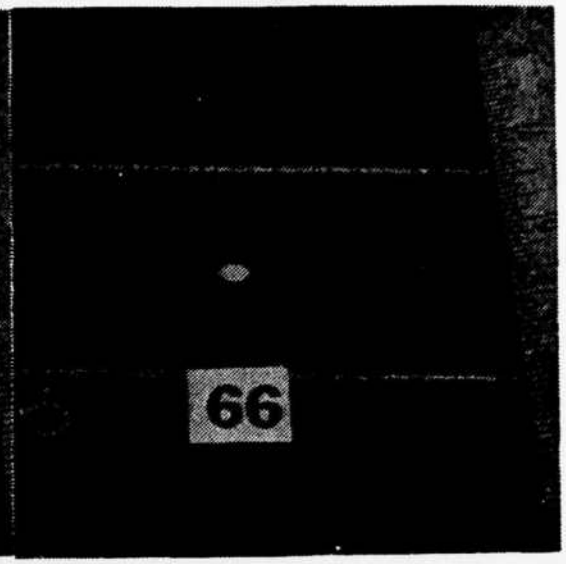


(H) a=2", 8-ply rib specimen, line loaded, $P_f$ = 1235 lbs.

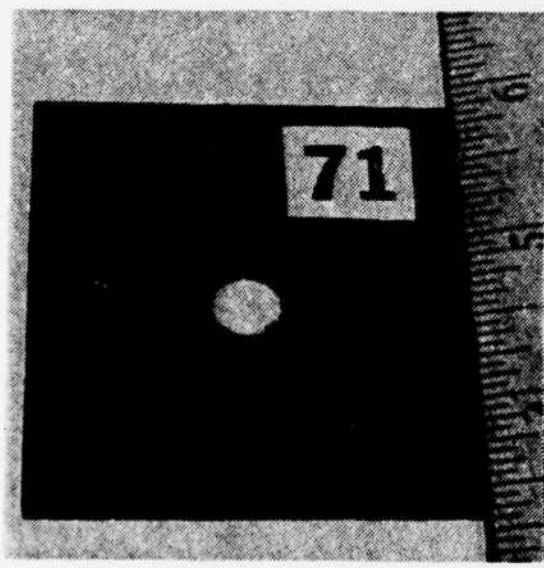


(I) through-plane shear, small moment, 16-ply, $P_f$ = 2925 lbs.

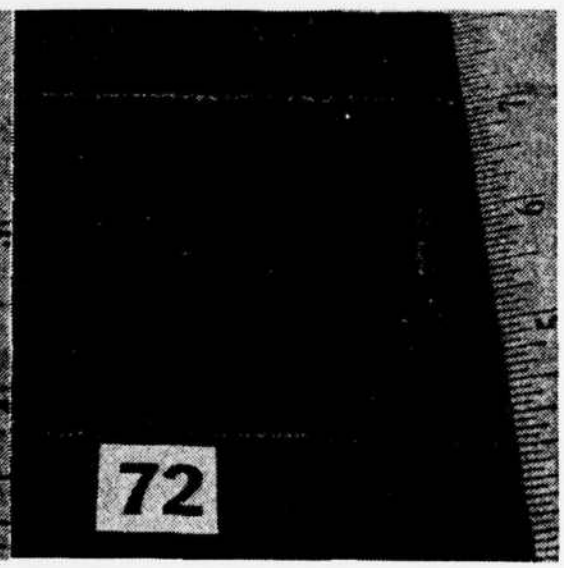


(J) a=3", 16-ply rib specimen, $P_f$ = 1255 lbs.

Figure 20 (cont'd)

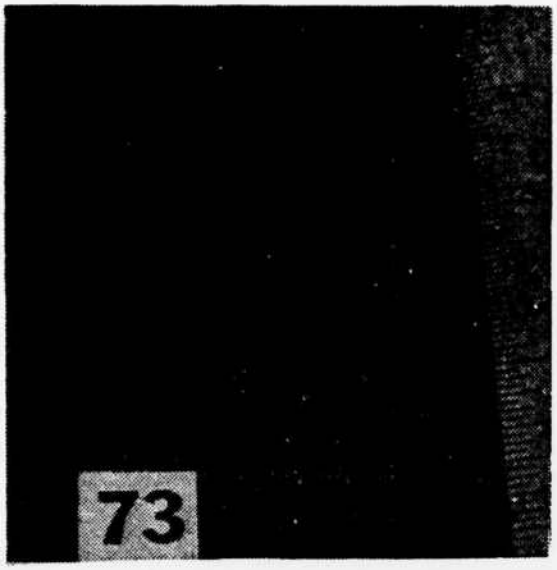


(K) a = 4", 16-ply rib specimen, $P_f$ = 1140 lbs.

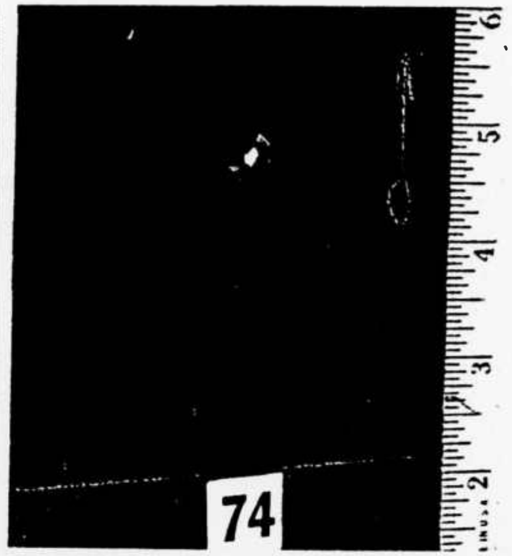


(L) a = 5", 16-ply rib specimen, $P_f$ = 1085 lbs.

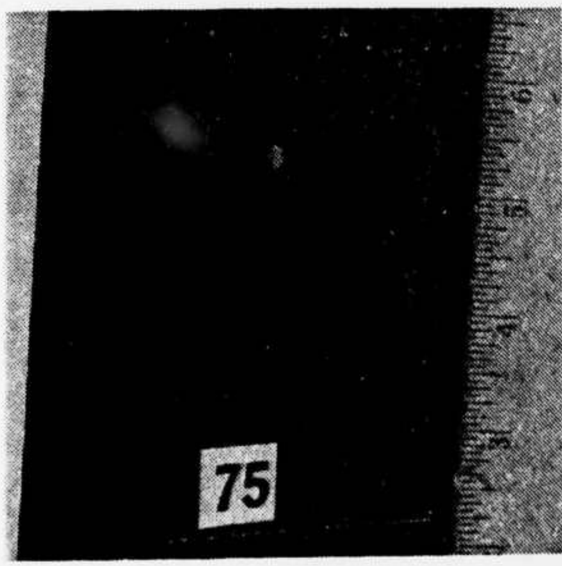


(M) a = 6", 16-ply rib specimen, $P_f$ = 985 lbs.

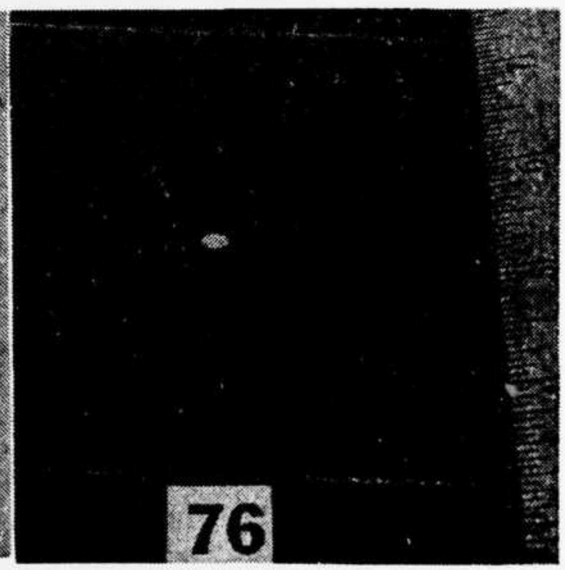


(N) a = 4", 16-ply rib specimen, line loaded, $P_f$ = 1780 lbs.

Figure 20 (cont'd)

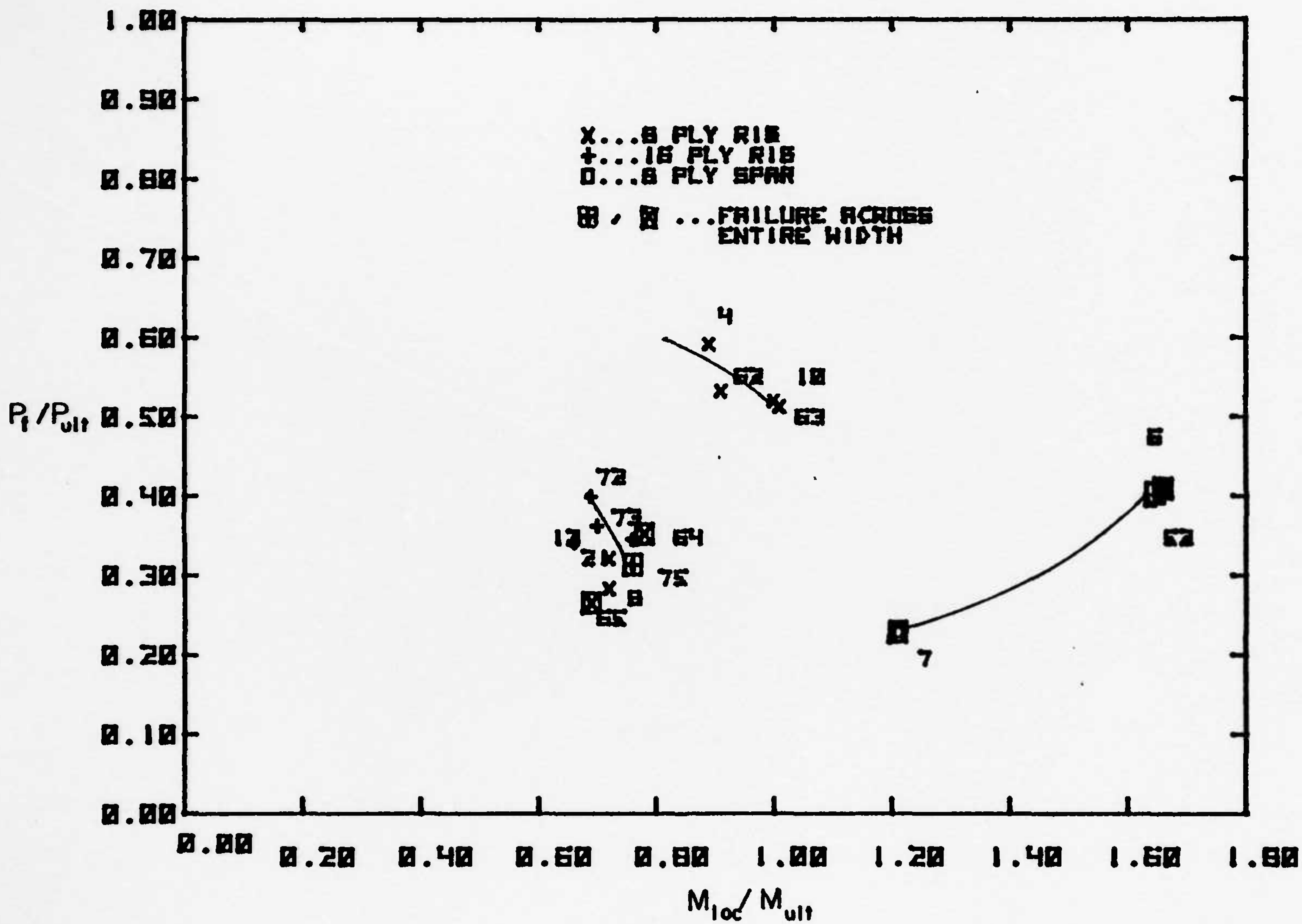
X...8 PLY RIB
+...16 PLY RIB
□...8 PLY SPAR
⊞ , ⊠ ...FAILURE ACROSS ENTIRE WIDTH
$P_f/P_{ult}$
$M_{loc}/M_{ult}$
1.00
0.90
0.80
0.70
0.60
0.50
0.40
0.30
0.20
0.10
0.00
0.20
0.40
0.60
0.80
1.00
1.20
1.40
1.60
1.80

Figure 21A

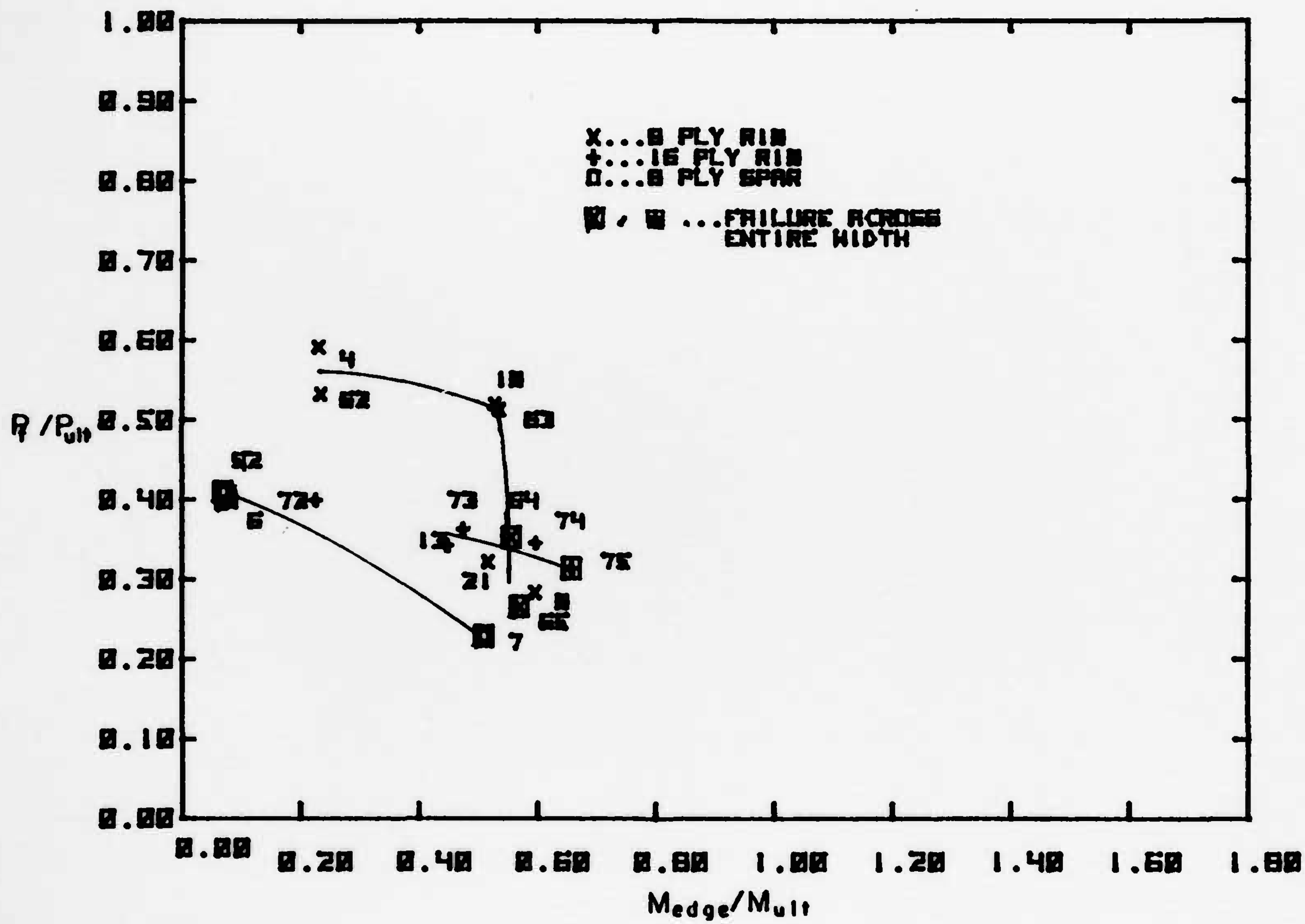
X...8 PLY RIB
+...16 PLY RIB
□...8 PLY SPAR
... FAILURE ACROSS ENTIRE WIDTH
1.00
0.90
0.80
0.70
0.60
0.50
0.40
0.30
0.20
0.10
0.00
0.20
0.40
0.60
0.80
1.00
1.20
1.40
1.60
1.80
$P_f / P_{ult}$
$M_{edge}/M_{ult}$

Figure 21B

## LIST OF REFERENCES


1. McDonnell Aircraft Company, Report MDCA3960, F-18 A/B, TF-18A/B Structural Description, by A. H. Baker, pp. 1-4, 29-46, 22 May 1976.

2. NAVAIR Air Development Center Report NADC-76249-30, Composite Wing Design for Advanced Harrier, by K. V. Stanberg, et al, pp. 9-30, March 1976.

3. Weinberger, R.A., Somoroff, A.R., Riley, B.L., U.S.Navy Certification of Composite Wings for the F-18 and Advanced Harrier Aircraft, advance copy of paper presented to AIAA Journal for publication, March, 1977.

4. Duva, A.N., Hydraulic Ram Effect on Composite Fuel Cell Entry Walls, M.S.Ae Thesis, Naval Postgraduate School, Monterey, 1976.

5. Advanced Composites Design Guide, Vol. I, Rockwell International Corporation, 1973.

6. Naval Postgraduate School Report 57Bp76051, Structural Response of Fluid-Containing-Tanks to Penetrating Projectiles (Hydraulic Ram) - A Comparison of Experimental and Analytical Results, by R.E. Ball, pp.2-3, May 1976.

7. Dynamic Science Report 1560-74-43, Tests of Hydraulic Ram Buffering Materials, by R.J. Dewitt and D. H. Zabel, pp. 8-105, 30 May 1974.

8. Aircraft Industries Association of America, Inc., National Aircraft Standard G18, Fastener-Recommended Shank, Hole, and Head to Shank Filler Radius Limits for, 1958.

9. Hercules, Incorporated, Graphite Materials, Data Summary Prepreg Type AS/3501-6, pp. 2-7, April 1976.

10. Advanced Composites Design Guide, Vol. II, Rockwell International, 1973.

11. Timoshenko, S. and Woinowsky-Krieger, S., Theory of Plates and Shells, 2d ed., pp. 135-137, McGraw-Hill, 1959.

12. Hodge, P.G., Plastic Analysis of Structures, pp. 10-30, McGraw-Hill, 1959.

13. Przemieniecki, J.S., Theory of Matrix Structural Analysis, McGraw-Hill, 1968.

14. Clough, R.W., Comparison of Three Dimensional Finite Elements, Keynote address presented at American Society of Civil Engineers Symposium, Nashville, Tennessee, 13-14 November 1969.

15. Bathe, K. J., ADINA, Acoustics and Vibration Laboratory, Massachusetts Institute of Technology, Cambridge, Massachusetts, September 1975.

16. Ball, R. E., "A Geometrically Nonlinear Analysis of Arbitrarily Loaded Shells of Revolution," NASA CR-909, January 1968.

## INITIAL DISTRIBUTION LIST

| | | No. of copies. |
|---|---|---|
| 1. | Defense Documentation Center<br>Cameron Station<br>Alexandria, Virginia 22314 | 2 |
| 2. | Library, Code 0142<br>Naval Postgraduate School<br>Monterey, California 93940 | 2 |
| 3. | Department Chairman, Code 67<br>Department of Aeronautics<br>Naval Postgraduate School<br>Monterey, California 93940 | 1 |
| 4. | Associate Professor R. E. Ball, Code 67Bp<br>Department of Aeronautics<br>Naval Postgraduate School<br>Monterey, California 93940 | 6 |
| 5. | Mr. J. G. Wilcox<br>Hi-Shear Corporation<br>2600 Skypark Drive<br>Torrance, California 90509 | 1 |
| 6. | LT Robert Norman Freedman, USN<br>TH #40, English Village<br>North Wales, Pennsylvania 19454 | 1 |

DATE
FILMED
-7